Methylotrophic methanogenesis in the Archaeoglobi revealed by cultivation of *Ca.* Methanoglobus hypatiae from a Yellowstone hot spring

Mackenzie M. Lynes[1], Zackary J. Jay[1], Anthony J. Kohtz[1], Roland Hatzenpichler[1,2,*]

[1] Department of Chemistry and Biochemistry, Center for Biofilm Engineering, and Thermal Biology Institute, Montana State University, Bozeman, MT 59717, USA

[2] Department of Microbiology and Cell Biology, Montana State University, Bozeman, MT 59717, USA

[*] Corresponding author: Roland Hatzenpichler, email: roland.hatzenpichler@montana.edu, 111 Chemistry and Biochemistry Building, Montana State University, MT-59718, Bozeman, USA

ORCID Numbers of Authors: M.M.L., 0000-0002-9410-0285; Z.J.J., 0000-0003-3062-4933; A.J.K., 0000-0002-0561-8710; R.H, 0000-0002-5489-3444

Running title: *Ca.* Methanoglobus hypatiae

Abstract

Over the past decade, environmental metagenomics and PCR-based marker gene surveys have revealed that several lineages beyond just a few well-established groups within the Euryarchaeota superphylum harbor the genetic potential for methanogenesis. One of these groups are the Archaeoglobi, a class of thermophilic euryarchaeotes that have long been considered to live non-methanogenic lifestyles. Here, we enriched *Candidatus* Methanoglobus hypatiae, a methanogen affiliated with the family Archaeoglobaceae, from a hot spring in Yellowstone National Park. The enrichment is sediment-free, grows at 64-70 ºC and a pH of 7.8, and produces methane from mono-, di-, and tri-methylamine. *Ca.* M. hypatiae is represented by a 1.62 Mb metagenome-assembled genome with an estimated completeness of 100% and accounts for up to 67% of cells in the culture according to fluorescence *in situ* hybridization. Via genome-resolved metatranscriptomics and stable isotope tracing, we demonstrate that *Ca.* M. hypatiae expresses methylotrophic methanogenesis and energy-conserving pathways for reducing monomethylamine to methane. The detection of Archaeoglobi populations related to *Ca.* M. hypatiae in 36 geochemically diverse geothermal sites within Yellowstone National Park, as revealed through the examination of previously published gene amplicon datasets, implies a previously underestimated contribution to anaerobic carbon cycling in extreme ecosystems.

Keywords: archaea, MCR, methane, stable isotope tracing, thermophile, transcriptomics

Introduction

Methanogenesis is one of the most ancient metabolic pathways and plays a major role in the biogeochemical carbon cycle. Phylogenomic reconstructions and geological evidence suggest that methanogenesis was among the earliest metabolisms to evolve and that the last common ancestor of all extant archaea likely was a methanogen (1-9). Therefore, the study of methanogens is essential for understanding the co-evolution of life and the biosphere. Methanogenic archaea are the primary producers of biogenic methane (CH_4) and contribute approximately 60% to the estimated 576 Tg of annual global methane emissions to the atmosphere (10, 11). Methanogenic pathways are classified by their carbon and electron sources (12-14). All methanogenic pathways converge at the terminal methane-forming step catalyzed by the methyl-coenzyme M reductase (MCR) complex. MCR and its homologs also catalyze the reverse reaction in the anaerobic oxidation of alkanes in alkanotrophic archaea (15, 16). MCR is uniquely present in all methanogens and is commonly used to identify potential methane and/or alkane cycling archaea in sequencing surveys (12, 17).

The physiology and biochemistry of methanogens has near-exclusively been investigated in axenic cultures of microorganisms belonging to the Euryarchaeota superphylum (12, 17-19). These predominantly grow by acetoclastic or CO_2-reducing hydrogenotrophic methanogenesis, with only rare observations of Euryarchaeotal methyl-reducing methanogens (12, 20, 21). As a result, despite the dominance of methyl-based methanogenesis in anoxic environments with high salt and/or high sulfate concentration (*e.g.*, anoxic marine sediments, coastal wetlands, hypersaline lakes), methylotrophic methanogenesis has in the past often been considered to be of comparatively limited environmental distribution. The extensive use of environmental metagenomics has led to the discovery of metagenome-assembled genomes (MAGs) encoding MCR from new lineages that are prevalent in anoxic environments, both within and outside the Euryarchaeota (2, 12, 22-26).

The majority of MAGs affiliated with archaeal phyla outside the Euryarchaeota are predicted to be methyl-reducing methanogens, with the exception of *Candidatus* (*Ca.*) Nezhaarchaeota (25, 27) and *Ca.* Methanomixophus affiliated with the order Archaeoglobales, which have been hypothesized to be CO_2-reducing hydrogenotrophic methanogens (12, 25, 28). This result is consistent with the observation that methylated methanogenic substrates, including methylamines and methanol, are prevalent in the environment, although their concentrations in hot springs is currently unknown. Further, methyl-reducing methanogenesis is considered the predominant mode of methanogenesis in anoxic marine, freshwater, and hypersaline sediments (reviewed in (20)).

Members of the class Archaeoglobi have long been considered non-methanogenic with isolates characterized as dissimilatory sulfate reducers brought into culture as early as 1987 (29). To date, only nine species of the class Archaeoglobi have been obtained in axenic culture, and all were sourced from marine

hydrothermal systems or off-shore oil reservoirs (30). The discovery of both MCR (25, 31, 32) and methyl-H_4M(S)PT:coenzyme M methyltransferase (MTR) complexes in genomes of the Archaeoglobaceae have suggested that members of this family may live by methanogenesis (28).

Very recently, important progress towards experimental verification of methanogenesis by members of this family has been made. Liu *et al.* reported the *in situ* expression of genes related to hydrogen-dependent methylotrophic methanogenesis and heterotrophic fermentation within populations of Archaeoglobi in a high-temperature oil reservoir (28). Lynes, Krukenberg *et al.* reported that Archaeoglobi can be enriched in hot spring mesocosms under methanogenic conditions (33). Wang *et al.* reported that *mcrABG* and other methanogenesis marker genes encoded by two Archaeoglobales MAGs were highly expressed in hot spring microcosms incubated at 65 ºC and 75 ºC (34). Importantly, one of these Archaeoglobales MAGs represented the only Mcr-encoding archaeon that expressed *mcrABG* genes in methanogenic microcosms performed without substrate addition or with the addition of 10 mM methanol at 75 ºC. This indirectly demonstrated the methanogenic nature of this archaeon (34). Last, Buessecker *et al.* reported the establishment of a methanogenic enrichment culture of *Ca.* Methanoglobus nevadensis from Great Boiling Spring (NV, USA) (35). The culture yields up to 158 µM methane after two weeks of incubation at its optimal growth temperature of 75 ºC. *Ca.* M. nevadensis is represented by a 63% complete MAG obtained from the culture and a 98% complete MAG obtained a decade earlier (35).

Here, we report on the enrichment cultivation of *Ca.* Methanoglobus hypatiae LCB24, a methanogen affiliated with the family Archaeoglobaceae, from a hot spring in Yellowstone National Park (YNP). Using a combination of targeted cultivation, growth experiments, microscopy, stable isotope tracing, metagenomics, and metatranscriptomics, we demonstrate that *Ca.* M. hypatiae lives by methylotrophic methanogenesis and converts different methylamines to methane. By examining previously published datasets for the presence of Mcr-encoding Archaeoglobi, we demonstrate that these archaea are distributed in geothermal features of YNP, where they likely contribute to anaerobic carbon cycling. Our study presents direct evidence of methanogenesis within the Archaeoglobaceae and adds to the growing body of evidence demonstrating that methanogenesis is widely spread within the Euryarchaeota superphylum.

Materials and Methods

All chemicals used in this study were sourced from Sigma Aldrich unless otherwise specified.

Sample Collection, Enrichment, and Cultivation

In November 2021, a slurry of sediment and water (1:9) was collected from an unnamed hot spring in the Lower Culex Basin of Yellowstone National Park (YNP), WY, USA. In our previous survey of Mcr-encoding archaea in YNP (33), this hot spring was given the identifier LCB024 (44.573294, -110.795388;

102 pH 7.8, 67 ˚C). A mixture of surface sediment (~1-2 cm deep) and hot spring water was collected into a
103 glass bottle and sealed headspace-free with a thick butyl rubber stopper. Collected material was transported
104 back to the lab and stored at room temperature. Using this material as inoculum, 30 mL enrichments were
105 established in February 2022 in 60 mL serum bottles. Material was homogenized by mixing and was then
106 diluted 1:10 (v/v) with anoxic medium in an anoxic glove box ($N_2/CO_2/H_2$; 90/5/5%).

107 Medium was prepared anoxically as described previously (36). Basal mineral medium contained a
108 base of (per liter): KH_2PO_4, 0.5 g; $MgSO_4 \cdot 7H_2O$, 0.4 g; NaCl, 0.5 g; NH_4Cl, 0.4 g; $CaCl_2 \cdot 2H_2O$, 0.05 g;
109 HEPES, 2.38 g; yeast extract, 0.1 g; and 0.002% (w/v) $(NH_4)_2Fe(SO_4)_2 \cdot 6H_2O$. Medium was transferred to
110 a Duran flask with a side opening and autoclaved for 20 m at 121 ˚C. Medium was then further
111 supplemented with 5 mM $NaHCO_3$, 1 mL trace element solution SL-10, 1 mL Selenite-Tungstate solution,
112 1 mL CCM vitamins (37), 0.0005% (w/v) resazurin, 10 mg of coenzyme-M, 2 mg sodium dithionite, 1 mM
113 dithiothreitol, 1 mM $Na_2S \cdot 9H_2O$, with pH adjusted to 7.8 using sodium hydroxide (NaOH, 12 N). Serum
114 bottles were sealed with butyl rubber stoppers and aluminum crimps before the headspace was exchanged
115 with N_2 (99.999%) for 5 minutes and set to a 200 kPa N_2 atmosphere. Monomethylamine (MMA) was added
116 from a filter-sterilized methylamine-hydrochloride anoxic stock solution to a final concentration of 10 mM.
117 The bacterial antibiotics streptomycin (50 mg/L; inhibitor of protein synthesis) and vancomycin (50 mg/L;
118 inhibitor of peptidoglycan synthesis) were added from filter-sterilized anoxic stock solutions. The
119 enrichments were incubated at 70 ˚C in the dark without shaking. Cultures were maintained by regular
120 transfer of 10% v/v into fresh media, which contained MMA and antibiotics. A sediment-free culture was
121 obtained after the third transfer after which it was transferred at 10% v/v to 50 mL in 125 mL serum bottles.
122

123 **Stable Isotope Tracing**

124 The conversion of ^{13}C- or D_3-MMA ($^{13}CH_3$-NH_2, CD_3-NH_2) to $^{13}CH_4$ or CD_3H was tracked by
125 incubating active enrichment cultures in the presence of 20% labeled substrate (98%; Cambridge Isotope
126 Laboratories). Incubations were carried out in 30 mL culture volumes in 60 mL serum bottles with 8% v/v
127 inoculum, 50 mg/L streptomycin, 50 mg/L vancomycin, 10 mM MMA, and N_2 gas (99.999%) incubated in
128 anoxic media (pH 7.8, 70 ˚C) in six replicates (SI Appendix, Fig. S3). Duplicate control incubations
129 included (i) ^{12}C-MMA and (ii) inoculum without MMA. Triplicate control incubations were performed with
130 (iii) ^{12}C-MMA plus 10 mM bromoethanesulfonate (BES) added in mid-exponential phase (day 33) to inhibit
131 methanogenesis and (iv) 10 mM BES added at time of inoculation (day 0) without substrate. Headspace
132 samples were collected throughout the experiment as described above and analyzed using a Shimadzu
133 QP2020 NX GCMS equipped with a GS-CarbonPLOT column (30 m × 0.35 mm; 1.5 µm film thickness;
134 Agilent) and operated in Selected Ion Monitoring mode. The instrument was operated using the method
135 described in Ai et al., 2013 (38) with helium as a carrier gas. All injections were performed by a Shimadzu

136 AOC-6000 autosampler robot. Peak areas corresponding to m/z ratios of 16 for $^{12}CH_4$, 17 for $^{13}CH_4$, and 19
137 for CD_3H were used for quantification.
138
139 **Metagenomic Sequencing, Assembly, and Annotation**
140 Two metagenomes were obtained over the course of this study. A 42 mL aliquot of the fourth transfer
141 of the enrichment (Fig. 1 T4-MG) was filtered onto a 0.22 µm filter. The filter was transferred to a lysing
142 matrix E tube and DNA extracted immediately following filtration. Genomic DNA was extracted using the
143 FastDNA Spin Kit for Soil (MP Biomedicals, Irvine, CA) following the manufacturer's guidelines.
144 A second metagenome was recovered from one of the six culture replicates grown in the presence of
145 CD_3-NH_2 and used for recruiting transcriptomic reads from the other replicates (Fig. 1 SIT-MG). A 60 mL
146 syringe flushed with N_2 gas was used to transfer 30 mL of culture to a sterilized oak ridge tube. Cells were
147 harvested through centrifugation for 30 minutes at 10,000 rpm at 4 ˚C. The supernatant was removed, and
148 DNA extracted from the pellet using the FastDNA Spin Kit for Soil (MP Biomedicals, Irvine, CA)
149 following the manufacturer's guidelines. Genomic DNA for both metagenomes was shipped to SeqCenter
150 (Pittsburgh, PA) and sample libraries were prepared using the Illumina DNA Prep kit and 10 bp unique
151 dual indices (UDI). The first metagenome (T4-MG) was sequenced on a NextSeq 2000 System (Illumina)
152 and the second (SIT-MG) sequenced on a NovaSeq 6000 System (Illumina), each producing 2x151 bp
153 reads. Demultiplexing, quality control, and adapter trimming was performed with bcl-convert v3.9.3.
154 Quality of the reads were evaluated with FastQC before quality, linker and adapter trimming, artifact and
155 common contaminant removal, and error correction were performed with the rqcfilter2 pipeline (maxn=3,
156 maq=10, trimq=20) and bbcms (mincount=2, hcf=0.6). Resulting reads were assembled with SPAdes
157 v3.15.13 (Nurk, 2017) (-k 33,55,77,99,127 --meta –only-assembler) and coverage was determined with
158 bbmap v38.94 (ambiguous=random) (https://sourceforge.net/projects/bbmap) (39). In addition to the initial
159 assembly, co-assemblies using both T4-MG and SIT-MG metagenomes were also performed (1) with reads
160 directly fed into SPAdes with the –only-assembler option excluded; and (2) with the trimmed and error
161 corrected reads and the same SPAdes parameters as above. The statistics of MAGs generated through
162 various assembly and quality control methods were evaluated, and the approach that produced the highest
163 quality MAG was chosen for subsequent analysis (Dataset S1). Quality was determined by considering
164 factors such as the number of resulting sequences, total length, completeness, and the minimum, maximum,
165 and average sequence lengths. Annotation of the assembled sequences was performed with Prokka v1.14.16
166 (40). Assembled scaffolds ≥2000 bp were binned using Maxbin v2.2.7 (41), Metabat v2.12.1 (with and
167 without coverage) (42), Concoct v1.0.0 (43), Autometa v1 (bacterial and archaeal modes with the machine
168 learning step) (44), followed by bin refinement with DAS_Tool v1.1.6 (45), as previously described (46).
169 Bin completeness and redundancy were assessed with CheckM v1.2.2 (47).

170

171 **RNA Extraction, Sequencing, and Transcriptomic Processing**

172 Total RNA was extracted for transcriptomics from four of the six replicates of Archaeoglobus cultivated in
173 the presence of labeled substrate ($^{13}CH_3$-NH_2 or CD_3-NH_2) for a total of eight replicates. Each replicate
174 culture in the exponential growth phase (day 32) was moved from the 70 ˚C incubator to an ice bath placed
175 at -20 ˚C for 40 minutes to stop cellular activity. A 60 mL syringe flushed with N_2 gas was used to transfer
176 30 mL of culture to a sterilized oak ridge tube and kept on ice. Cells were harvested through centrifugation
177 for 30 minutes at 10,000 rpm at 4 ˚C. The supernatant was removed, and the pellet transferred to a lysing
178 matrix E tube (MP Biomedicals, Irvine, CA) to which 600 µL of RNA lysis buffer was added. Samples
179 were homogenized in a MP Bioscience FastPrep instrument for 40 seconds at a speed setting of 6.0 m/s
180 followed by centrifugation for 15 minutes at 14,000 rpm. RNA was extracted using the Quick-RNA
181 miniprep kit (Zymo Research, Irvine, CA) including a DNAse treatment step and eluted in 50 µL of RNAse
182 free water. Centrifugation steps were performed at 15,000 rpm and the final spin for elution at 10,000 rpm.
183 Of the eight replicates extracted, six measured >50 ng/µL (3x $^{13}CH_3$-NH_2 and 3x CD_3-NH_2) and were sent
184 for transcriptomic sequencing at SeqCenter (Pittsburgh, PA). Samples were DNAse treated with Invitrogen
185 DNAse (RNAse free). Library preparation was performed using Illumina's Stranded Total RNA Prep
186 Ligation with Ribo-Zero Plus kit and 10bp UDI. Sequencing was done on a NovaSeq 6000, producing
187 paired end 151bp reads. Demultiplexing, quality control, and adapter trimming was performed with bcl-
188 convert (v4.1.5). Read quality was further evaluated with FastQC v0.11.9 (48) before quality trimming and
189 artifact, rRNA, and common contaminant removal with the rqcfilter2 pipeline (trimq=28, maxns=3,
190 maq=20), and error correction with bbcms (mincount=2, hcf=0.6) from the BBTools suite v38.94 (39).
191 Additional rRNA gene reads were detected and removed with Ribodetector v0.2.7 (49) and any remaining
192 rRNA gene reads were finally removed with bbmap, using rRNA genes recovered from the metagenomes
193 (see below) as references. The resulting mRNA reads were mapped against annotated genes from the paired
194 metagenomes with bbmap to calculate RPKM (ambig=random).

195

196 **Data Availability**

197 All metagenomic, metatranscriptomic, and amplicon data discussed in this manuscript are available
198 under NCBI BioProject ID PRJNA1014417. McrA gene amplicon data from YNP hot springs discussed in
199 this manuscript has been previously published (Lynes et al., 2023) and is available under NCBI under
200 BioProject PRJNA859922.

201

202 **<u>Results and Discussion</u>**

203 **Cultivation**

204 In our recent survey on the diversity of Mcr-encoding archaea in the geothermal features of YNP,
205 mesocosms seeded with biomass from a hot spring located within the Lower Culex Basin (LCB024; pH 7-
206 8, 56-74 ˚C), had shown potential to enrich for methanogenic Archaeoglobi (33). Using a sediment slurry
207 collected from LCB024, we initiated incubations supplied with monomethylamine (MMA) and antibiotics
208 incubated in anoxic media (pH 7.8, 70 ˚C) under a N_2 headspace. The relative abundance, as determined by
209 16S rRNA gene amplicon sequencing, of Archaeoglobi-affiliated organisms in LCB024 was 0.32% in the
210 initial slurry and had fallen to 0.02% by the time incubations were initiated a few months after samples had
211 been collected (Fig. 1A).
212 Methane was detected after 36 days in the initial enrichment and the culture transferred to fresh media
213 after reaching the late exponential phase of methane production following 70 days of incubation (447 µM;
214 Fig. 1B). Five Archaeoglobi related 16S rRNA gene amplicon ASVs were identified in the initial
215 enrichment, however one ASV grew to dominate the microbial community after the first transfer and
216 reached 74.8% relative abundance after 62 days. In the transfers that followed, Archaeoglobi-related
217 sequences became the only archaeal reads detected by 16S rRNA gene amplicon sequencing with the
218 second most abundant organism a bacterium affiliated with the *Pseudothermotoga* at 6.8%. Although the
219 CO_2-reducing methanogen *Methanothermobacter* sp. was detected at 0.45% relative abundance in the
220 slurry material used for inoculation, it was not detected in any subsequent transfers, nor were any known
221 methanogens. Over subsequent transfers (238 days, T2-T5), the relative abundance of Archaeoglobi ASVs
222 ranged from 46 to 69% and the final methane yield steadily increased from 1,844 to 2,459 µM. A sediment-
223 free enrichment was obtained by the third transfer. Starting with the fourth transfer, the culture volume was
224 scaled from 30 mL to 50 mL. By the sixth transfer, the culture produced 3,943 µM methane within 34 days.
225 Metagenomic sequencing at two timepoints (day 335 of the enrichment and day 33 of the isotope tracing
226 experiment described below) and 16S rRNA gene amplicon sequencing over recurring transfers (Fig. 1A)
227 demonstrated that ASVs and MAGs affiliated with Archaeoglobi represented the only archaeon in culture
228 LCB24. A single MCR complex (*mcrAGCDB*) belonging to the Archaeoglobi MAG was present, indicating
229 this MAG represents the only methanogenic population.
230
231 **Metagenomics and Phylogenetics**
232 The reconstructed Mcr-encoding Archaeoglobi MAG from culture LCB24 was 1.62 Mbp in length
233 with an estimated completeness of 100% according to checkM (SI Appendix, Table S3). This MAG was
234 the result of a combined assembly of the T4-MG and SIT-MG metagenomes as this method yielded an
235 improved assembly. Therefore, it was used for phylogenomic analysis against Archaeoglobi reference
236 MAGs and genomes using 33 conserved single copy marker proteins and 16S rRNA genes (Fig. 2AB, SI
237 Appendix, Table S4). The phylogenomic analysis showed that MAGs encoding MCR complexes clustered

separately from those lacking *mcr* gene sequences. Consistently, 16S rRNA gene phylogeny supported this clustering with a pronounced separation of hot spring reference genomes and MAGs from current known isolates of Archaeoglobi, resulting in three main clusters: (i) those retrieved from North American hot springs (YNP and Great Boiling Spring, GBS), (ii) those originating from hot springs in China, and (iii) isolates, all of which were obtained from deep-sea marine hydrothermal systems (Fig. 2B).

LCB24 and closely related reference MAGs and isolate genomes exhibited a range of amino acid identities (AAI, 52.6-98.6%; Fig. 2C). Altogether, the LCB24 MAG was found to be highly related to previously obtained Archaeoglobi MAGs encoding the MCR complex and only distantly related to other Archaeoglobales sp. ~~confirmed sulfate-reducing Archaeoglobales~~ (AAI, 58.9-65%; ANI, 70.3-70.6%; 16S rRNA ANI, 91.6-93.8%; SI Appendix Fig. S1, S2). Based on AAI, MAG LCB24 was most closely related to Archaeoglobi LCB024-003 MAG (AAI, 98.6%), which we had obtained from the same hot spring in a previous study (33). The ANI and AAI values to the closest cultured methanogen, *Ca.* Methanoglobus nevadensis GBS, are 80.2 and 83.3%, respectively. Based on these results, we designate this archaeon *Ca.* Methanoglobus hypatiae strain LCB24, named after the philosopher Hypatia of Alexandria (for a protologue, see the SI Appendix, Results and Discussion). The estimated relative abundance of *Ca.* M. hypatiae based on the SIT-MG was 92.8%. Other community members in the LCB24 culture with >1% relative sequence abundance included members of the *Pseudothermotoga* (3.2%), *Desulfovirgula* (1.7%), and the family Moorellaceae (1.3%) (Fig. 1A, Dataset S1).

The only *mcrAGCDB* genes recovered from both metagenomes belong to the genome of *Ca.* M. hypatiae. Phylogenetic analysis of the single copy of McrA indicated its close relationship to McrA sequences found in members of the TACK superphylum (Fig. 2D). This contrasts with the placement of *Ca.* M. hypatiae within the Euryarchaeota based on phylogenomics (Fig. 2A), suggesting that Archaeoglobi could have obtained the MCR complex as a result of a horizontal gene transfer event from an archaeon in the TACK superphylum (7, 8). Also, it could indicate that non-methanogenic Archaeoglobi lost the capacity for anaerobic methane cycling after they had diverged from a shared methanogenic ancestor.

Methanogenic Activity of *Ca.* M. hypatiae

To gain insight into the activity of *Ca.* M. hypatiae under methanogenic and non-methanogenic conditions, a stable isotope tracing (SIT) experiment was conducted. Cultures were incubated in the presence of 10 mM of MMA; 8 mM of substrate were isotopically light, whereas the remaining 2 mM consisted of either ^{13}C-monomethylamine ($^{13}CH_3$-NH_2) or D_3-monomethylamine (CD_3-NH_2). Addition of the methanogenesis inhibitor bromoethanesulfonate (BES) was used as a non-methanogenic control (Fig. 1B, 3, SI Appendix, Fig. S3). On average across six replicates, the cultured converted $^{13}CH_3$-NH_2 to 356 µM $^{13}CH_4$ (17.8%) and 138.71 µM $^{13}CO_2$ (6.9%) by day 32 (Fig. 3AC, Dataset S2). The conversion of CD_3-

272 NH_2 was nearly identical yielding 355 μM CD_3H (Fig. 3B). In the exponential phase of methane production,
273 five of the six replicates were harvested for metagenomic and metatranscriptomic sequencing while the
274 sixth replicate was allowed to grow to stationary phase. The replicate allowed to grow in each respective
275 experiment converted the provided $^{13}CH_3$-NH_2 to 717.7 μM $^{13}CH_4$ (35.9%) and 212.95 μM $^{13}CO_2$ (10.65%)
276 or CD_3-NH_2 to 394.76 μM CD_3H (19.7%) by day 38 (Fig. 3ABC). These results confirmed
277 monomethylamine was converted to methane by the LCB24 culture. The production of $^{13}CO_2$ may represent
278 the dismutation of $^{13}CH_3$-NH_2 to generate reducing power for methanogenesis via the methyl-branch of the
279 Wood-Ljungdahl pathway or may be explained by other organisms in the culture catabolizing MMA. Yet,
280 no transcriptomic evidence for this activity was present in this experiment. No methane production was
281 observed for cultures treated with BES or in cultures incubated without MMA (Fig. 3D). When BES was
282 added to cultures in the exponential phase, methane production ceased indicating the generation of methane
283 is reliant on the Archaeoglobi MCR (Fig. 3E).
284
285 **Visualization and Cell Enumeration**
286 The growth of *Ca.* M. hypatiae was tracked in four replicates during the SIT experiment with
287 catalyzed reporter deposition fluorescence *in situ* hybridization (CARD-FISH) using a general archaea-
288 targeted probe Arch915 (50) and DNA-staining (DAPI) (Fig. 1C). As the production of methane increased
289 throughout the experiment, there was a concurrent rise in the relative cell abundance of *Ca.* M. hypatiae
290 (Fig. 3F, SI Appendix, Table S5). The initial assessment on day 22 across four replicates revealed the total
291 cell density to be $3.45 \times 10^7 \pm 1.14 \times 10^7$ before substantial concentrations of methane had been detected in
292 the headspace (<132 μM). By day 32, methane concentrations reached 1,777±739 μM and the total cell
293 density increased to $6.97 \times 10^7 \pm 3.73 \times 10^7$ cells mL^{-1} with 54% (±9.6%) of cells labeled as *Ca.* M. hypatiae
294 (Fig. 3F). All but one of these replicates were then sacrificed for further analysis. Finally on day 45, the
295 remaining replicate reached a headspace methane concentration of 4,109 μM and a total cell density of 1.22
296 $\times 10^8$ with 53% of cells labeled as *Ca.* M. hypatiae.
297 Visualization of the enrichment culture via scanning electron microscopy (SEM) revealed that most
298 cells exhibited a regular to irregular coccoid morphology, with a width ranging from 0.5-1 μm (Fig. 1D).
299 This morphology has previously been described for other Archaeoglobi species (30, 51-53).
300
301 **Alternative Substrates and Temperature Optimum**
302 We determined the substrate and temperature range of *Ca.* M. hypatiae by growing the culture in the
303 presence of several substrates at 70 ºC or with 10 mM MMA at 60-85 ˚C (Fig. 4AB). Conditions that lead
304 to the production of methane included 10 mM trimethylamine (TMA), 10 mM dimethylamine (DMA), 10
305 mM MMA in media without yeast extract, and the control with 10 mM MMA and 0.01% yeast extract.

306 Methane production of cultures grown with MMA in the presence or absence of yeast extract were
307 indistinguishable (5,202±606 and 5,703±410 μM CH_4, respectively) indicating that yeast extract is not
308 essential for methanogenic growth. Observed methane concentrations were higher in incubations amended
309 with DMA (10,115±836 μM CH_4) and TMA (9,524±3,626 μM CH_4, with a wide range of 5,361-11,993
310 μM) on average more than the MMA controls, consistent with what has been observed for other
311 methylotrophic methanogens (54). Incubations amended with 10 mM methanol (MeOH) did not produce
312 methane after 47 days of incubation at 70 ˚C. Due to its use by sulfate reducing organisms as an electron
313 donor (55), 10 mM lactate (LAC) was tested, as well as 10 mM MMA with 10 mM LAC, but none of these
314 incubations produced methane. Production of methane has not been observed in any attempted transfers
315 where hydrogen (99.9999% purity) was present in the headspace, or hydrogen with MMA was added.
316 The enrichment grew optimally at both 64 and 70 ˚C with relative amounts of methane produced at
317 5,304±451 μM and 5,202±606 μM, respectively. This deviates from the predicted optimal growth
318 temperature of 74.4˚C, which was derived from the translation of proteins in the Ca. M. hypatiae MAG
319 using Tome (56). This is lower than the observed range of growth and optimum temperatures for type
320 strains of non-methanogenic Archaeoglobus which have been demonstrated to grow between 50 and 95 ˚C
321 with optimal temperatures between 75-83 ˚C in organisms sourced predominantly from deep sea vent
322 environments (30). No methane production was detected at temperatures 77 ˚C or above or lower than 64
323 ˚C after 47 days of incubation (Dataset S4).
324
325 **Genomic and Transcriptomic Basis for Methanogenesis**
326 The assembled metagenome obtained at the end of the SIT experiment was used to align a total of
327 23,376,154 metatranscriptome mRNA reads obtained from six replicates harvested in the exponential
328 growth phase and to create a detailed reconstruction of the metabolism of *Ca.* M. hypatiae (Fig. 3AB, 5,
329 Dataset S5). A total of 22,891,651 reads, *i.e.,* 97.8% of all recovered reads, were recruited to the *Ca.* M.
330 hypatiae MAG. Only 2.1% of the total mRNA reads (484,503) were aligned with other co-enriched
331 organisms. Among these, only 13 genes across four MAGs were expressed above 200 reads per kilobase
332 of transcript per million mapped reads (RPKM) and just five genes exceeded >1,000 RPKM. Genes required
333 for the conversion of methylamine to methane were among the top 2% of highest expressed genes
334 transcribed by *Ca.* M. hypatiae, including genes encoding the MCR complex (*mcrAGCDB*; 13,046-18,098
335 RPKM), one of three monomethylamine methyltransferase copies (*mtmB*; 9,884 RPKM), dimethylamine
336 corrinoid (*mtbC*; 3,677 RPKM), and methanol:coenzyme M methyltransferase (*mtaA*; 12,577 RPKM) (Fig.
337 5). Seven copies of substrate-specific methyltransferases for MMA (*mtmB*; 3 copies), DMA (*mtbB*; 2
338 copies), and TMA (*mttB*; 2 copies) were present in the genome, but methanol methyltransferase (*mtaB*) was
339 not identified. These genes were differentially expressed with one copy for each type of methylamine

340 expressed above 3,200 RPKM. In addition to *mtbC*, two gene copies of the trimethylamine corrinoid protein
341 (*mttC*) were found in the genome but their expression was relatively low (<460 RPKM average).
342 Monomethylamine corrinoid (*mtmC*) or methanol corrinoid (*mtaC*) proteins were not identified in *Ca.* M.
343 hypatiae. Additionally, genes were expressed for pyrrolysine synthesis (*pylBCD*; 819, 343, 37 RPKM) and
344 the methyltransferase corrinoid activation protein (*ramA*; 1,076 RPKM), both of which support
345 methylamine methyltransferases in methylotrophic methanogenesis (57, 58). The absence of *mtmC* and the
346 high expression levels of *mtbC* (3,677 RPKM) and *mtaA* (12,577 RPKM) suggest that they are responsible
347 for the transfer of a methyl group from monomethylamine to coenzyme M (CoM) after it has been
348 transferred by a substrate-specific methyltransferase (*mtmB*). Consistent with the observed methane
349 production from DMA and TMA, *Ca.* M. hypatiae can use these methylamines and expressed the
350 corresponding genes (*mtbB*, *mttB*) at comparatively high levels (JOOIALLP_01813 *mtbB* 3,249 RPKM;
351 JOOIALLP_01787 *mttB* 5,324 RPKM; Fig. 4B, 5). It is worth noting that the expression of mtbB/mttB was
352 detected despite the culture not having been previously exposed to DMA or TMA at the time of the
353 transcriptomics experiment. We hypothesize that *Ca.* M. hypatiae could employ one of two strategies: it
354 either (i) constitutively expresses all substrate-specific methyltransferases and corrinoid proteins as a
355 precautionary measure to accommodate substrates potentially encountered *in situ*, or (ii) *Ca.* M. hypatiae
356 transcriptionally co-regulates the genes responsible for these functions.

357 *Ca.* M. hypatiae expressed the methyl-branch of the Wood-Ljungdahl pathway (WLP) and the acetyl-
358 CoA decarbonylase/synthase complex (Cdh, *cdhABCDE*), which is consistent with genes observed and
359 shown to be expressed in sulfate-reducing Archaeoglobi genomes (55). This includes two paralogous copies
360 of 5,10-methylenetetrahydromethanopterin reductase (*mer*) which might function as a traditional Mer,
361 considering that these genes are also members of the large luciferase-like monooxygenase family
362 (pfam00296)(35). The expression of genes in the WLP varied. Methylenetetrahydromethanopterin
363 dehydrogenase (*mtd*), methenyltetrahydromethanopterin cyclohydrolase (*mch*), formylmethanofuran-
364 tetrahydromethanopterin N-formyltransferase (*ftr*), formylmethanofuran dehydrogenase (*fwdABC*), and
365 one copy of the *mer* homologs were expressed at comparatively high levels (456-2,763 RPKM), whereas
366 FwdDEFG and the other *mer* copy were only minimally expressed (<180 RPKM) (Dataset S5). The high
367 expression of the Cdh complex (*cdhACDE*; 3,063±362, *cdhB* 677 RPKM average across subunits) suggests
368 that *Ca.* M. hypatiae is capable of autotrophically fixing CO_2 to acetyl-CoA as has been shown for other
369 *Archaeoglobus* species (59). Acetyl-CoA could also be derived from the degradation of fatty acids present
370 in yeast extract through the process of beta-oxidation. Enzymes involved in this pathway were expressed at
371 moderate to high levels during growth (Dataset S6). Pyruvate synthase (Por) was highly expressed
372 providing a way for acetyl-CoA to be converted to pyruvate and subsequently be fed into major biosynthetic
373 pathways. Specifically, *Ca.* M. hypatiae encodes pyruvate carboxylase (PycAB), an incomplete reductive

374 tricarboxylic acid cycle (rTCA), phosphoenolpyruvate synthase (Pps), most enzymes needed for
375 gluconeogenesis, and several enzymes associated with the pentose phosphate pathway in archaea, which
376 were all expressed at varying levels (Dataset S5). Together, these pathways provide *Ca.* M. hypatiae the
377 capacity to synthesize amino acids, carbohydrates, integral components of the cell wall, and vital sugars for
378 nucleic acids.

379 Several complexes related to energy conservation and electron transport were moderately to highly
380 expressed. *Ca.* M. hypatiae encodes a fused heterodisulfide reductase (*hdrDE*) that was highly expressed
381 (1,106±120 RPKM) in addition to a fused *hdrD/mvhD* and four copies of *hdrD* that were all expressed at
382 much lower levels (<500 RPKM). The differing levels of transcription suggest the membrane-bound HdrDE
383 is responsible for the regeneration of coenzymes M and B through the reduction of heterodisulfide (CoM-
384 S-S-CoB). Additionally, the absence of HdrB, which contains the active site for disulfide reduction,
385 eliminates the possibility that disulfide reduction could occur via a HdrABC complex (60). As reported for
386 *Ca*. M. nevadensis (35), a unique gene cluster was identified containing F_{420}-non-reducing hydrogenase
387 (MvhAGD), two HdrA copies and a QmoC fused to a HdrC. One HdrA copy (JOOIALLP_01710) was
388 predicted by DiSCo analysis as a quinone-modifying oxidoreductase (QmoB), a protein related to the HdrA
389 of methanogens (61, 62). This cluster was expressed at high levels (995-2,431 RPKM average), suggesting
390 its importance for electron transfer in *Ca.* M. hypatiae. We hypothesize these subunits are associating
391 together *in vivo* to bifurcate electrons from hydrogen (H_2) to reduce both menaquinone (MQ) and ferredoxin
392 (Fd_{ox}), as proposed recently (35, 63). Lastly, *Ca.* M. hypatiae moderately expressed a membrane-bound
393 $F_{420}H_2$:quinone oxidoreductase (Fqo) complex (88-280 RPKM across subunits) and a V-type ATP synthase
394 (24-442 RPKM across subunits).

395 The electrons required for reducing the CoM-S-S-CoB heterodisulfide could originate from two
396 possible routes. The first possibility would rely on sourcing electrons from hydrogen, which could be
397 oxidized by the Mvh-Qmo-Hdr complex coupled to menaquinone reduction. H_2 may be produced through
398 the activity of a group 3b [NiFe]-sulfhydrogenase (HydABDG), which was the highest expressed
399 hydrogenase complex with an average RPKM of 4,421 across subunits (64, 65). To evolve hydrogen via
400 HydABDG, reducing power, via NADPH, could be supplied by sulfide dehydrogenase (SudAB; SudA,
401 1,088 RPKM; SudB, 495 RPKM). Alternatively, NADPH could instead be provided to biosynthesis
402 pathways and therefore be decoupled from methanogenic metabolism. H_2 could also potentially be sourced
403 from fermentative bacteria in the enrichment culture, however, the low number of hydrogenases encoded
404 by co-enriched organisms were only very lowly expressed at the time of sampling for metatranscriptomics
405 (<51 RPKM). At this point, the source of H_2 *Ca.* M. hypatiae uses remains uncertain, as no H_2 was added
406 to the headspace. Second, in a hydrogen-independent electron transport system, reduced F_{420} and ferredoxin
407 could be produced through the dismutation of methylated substrate to CO_2 through the WLP. Reduced F_{420}

408 could be oxidized by the Fqo complex and contribute to a reduced menaquinone pool that could be used by
409 the fused HdrDE complex to reduce CoM-S-S-CoB. Reduced ferredoxin could be oxidized at a soluble
410 FqoF to reduce F_{420} or at an Fqo complex lacking FqoF to reduce menaquinone (66, 67). Based on the low
411 expression levels of the Fqo complex (171±67 RPKM) and the absence of F_{420}-reducing hydrogenase (*frh*)
412 from the genome, it is not likely the WLP runs in the reductive direction as a source of reduced F_{420} would
413 be required. Resolving the exact configuration of the electron transport system encoded by *Ca.* M. hypatiae
414 will require biochemical confirmation in future investigations.

415 Importantly, genes necessary for dissimilatory sulfate reduction typically observed in sulfate-
416 reducing members of the Archaeoglobi, including dissimilatory sulfite reductase (*dsrAB*), sulfate
417 adenylyltransferase (*sat*), and adenylylsulfate reductase (*aprAB*), were neither identified in the genome of
418 *Ca.* M. hypatiae nor in the unbinned fraction of the metagenome. They were also absent from the
419 comparatively incomplete MAG of *Ca.* M. nevadensis GBS (35). However, *Ca.* M. hypatiae encodes
420 subunits *dsrMK* and *dsrOP* of the Dsr complex in addition to *dsrC*. This complex is strictly conserved in
421 sulfate-reducing organisms (68) where it mediates electron transfer from the periplasm to the cytoplasm
422 reducing the disulfide bond found in DsrC cysteines (69). The expression of the Dsr complex and *dsrC* was
423 low (450±63 RPKM) during growth on monomethylamine suggesting it is not vital to the metabolism of
424 *Ca.* M. hypatiae. The presence of the Dsr complex, DsrC, and subunits QmoC and QmoB in the genome
425 may be explained as evolutionary remnants from ancestral Archaeoglobi, growing initially as sulfate-
426 reducing organisms but later transitioning to a methanogenic lifestyle (7, 8). This raises the question
427 whether intermediate of this process, Archaeoglobi capable of both methanogenesis and sulfate-reduction
428 (and possible anaerobic oxidation of methane), still exist today (25, 28).

429 Collectively, the metagenomic and transcriptomic data confirmed that *Ca.* M. hypatiae is not only
430 the sole archaeon but the sole methanogen in our culture. The metabolic reconstruction and
431 metatranscriptomic results are consistent with methylotrophic methanogenesis from methylamines. The
432 absence of genes required for sulfate reduction eliminates the possibility for this metabolism in *Ca.* M.
433 hypatiae. A unique gene cluster (Mvh-Qmo-Hdr) potentially involved in energy conservation was
434 expressed, however future studies will be required to test how *Ca.* M. hypatiae internally cycles electrons
435 for methanogenesis and if it sources H_2, or other reductants, from the medium or co-enriched bacteria.
436

437 **Distribution of *Ca.* Methanoglobus Across Geothermal Features in YNP**

438 16S rRNA and *mcrA* gene amplicon sequence data generated in a recent microbial diversity survey
439 of 100 geothermal features in YNP (33) were used to analyze the distribution of Archaeoglobi related to
440 *Ca.* M. hypatiae (SI Appendix, Fig. S5). 16S rRNA gene amplicons closely related to *Ca.* M. hypatiae
441 (96.7-100% sequence identity) were found in seven DNA samples from six hot springs (pH 5.1-9.35, 31-

442 78 ºC) in addition to hot spring LCB024 (the source of this culture) at relative abundances ranging from
443 0.02-0.22%. In addition, *mcrA* gene ASVs affiliated with Archaeoglobi were PCR-amplified from 53 DNA
444 samples, out of 201 total samples that had been screened by PCR. These 53 samples had been collected
445 from microbial mats or sediments originating from 36 geothermal features distributed across various
446 thermal regions within YNP by Lynes, Krukenberg *et al.* (33). Archaeoglobi-related *mcrA* genes were found
447 in geothermal features with a pH range of 2.61 to 9.32 and a temperature range of 18.4 ºC to 93.8 ºC.
448 Collectively, our results and the studies by Wang *et al*. and Buessecker *et al*., who reported that Mcr-
449 encoding Archaeoglobi are present (35) and transcriptionally active in hot spring mesocosms (34),
450 demonstrate the previously overlooked role that Archaeoglobi might play in the anaerobic carbon cycle of
451 geothermal environments.
452
453 **Conclusion**
454 In summary, the cultivation of *Ca.* Methanoglobus hypatiae LCB24 provides direct experimental
455 evidence that members of the Archaeoglobi are methanogens. *Ca.* M. hypatiae can use MMA, DMA, and
456 TMA as methanogenic substrates and grows optimally at 64-70 ºC, as evidenced by metagenomics,
457 metatranscriptomics, and isotope tracing experiments. Metagenomic sequencing and phylogenomic
458 analysis confirmed the close relationship of *Ca.* M. hypatiae to other Mcr-encoding Archaeoglobi and the
459 relatedness of its *mcrA* to MAGs of the TACK superphylum, some of which have recently been shown to
460 also be methanogens (70, 71). Together, this supports the idea that the capacity for methanogenesis is deeply
461 rooted in the archaea and possibly dates to the last common ancestor of archaea (1, 3, 7, 8, 72). The wide
462 distribution of Archaeoglobi-affiliated *mcrA* gene sequences and *Ca.* M. hypatiae-related 16S rRNA gene
463 sequences in geothermal features across YNP suggests that members of this lineage play a hitherto
464 unaccounted-for role in anaerobic carbon cycling in these extreme ecosystems. Future studies of *Ca.* M.
465 hypatiae and other methanogens will provide valuable insights into the evolution of methane metabolism
466 and the significance of these archaea in biogeochemical cycles across geothermal and other environments.
467
468 **Acknowledgements**
469 This study was funded through a NASA Exobiology program award (80NSSC19K1633) to R.H. We
470 thank the US National Park Service for permitting work in YNP under permit number YELL-SCI-8010.
471 We thank George Schaible (MSU) for help with SEM imaging, Dr. Viola Krukenberg (MSU) for initial
472 FISH methodology development, Sylvia Nupp, Dr. Andrew Montgomery, and Paige Schlegel (all MSU)
473 for assistance with field sampling, Dr. Christopher Lemon (MSU) for allowing use of his cooling centrifuge,
474 and Dr. Marike Palmer (UN Las Vegas) for discussing naming of this archaeon.
475

476 **Author Contributions**

477 M.M.L. and R.H. developed the research project. M.M.L., Z.J.J., A.J.K, and R.H. designed
478 experiments. M.M.L. and A.J.K. conducted field sampling. M.M.L. performed cultivation, extracted DNA
479 for amplicon and metagenomic sequencing, extracted RNA for transcriptomic sequencing, and conducted
480 physiology and stable isotope experiments. A.J.K. developed GC/GCMS protocols and processed GCMS
481 samples. Z.J.J. processed and annotated metagenomic and transcriptomic data, assembled MAGs, mapped
482 transcripts, assigned taxonomy, constructed 16S rRNA gene phylogeny, and performed phylogenetic
483 analysis of MAGs. M.M.L. conducted phylogenetic analysis of amplicon data, refined gene annotations,
484 reconstructed, and interpreted the metabolic potential of *Ca.* M. hypatiae with insight from Z.J.J and A.J.K.
485 R.H. was responsible for funding and supervision of the project. M.M.L. and R.H. wrote the manuscript,
486 which was then edited by all authors.

487

488 **Conflict of interest:** none declared.

References

1. Wolfe JM, Fournier GP. Horizontal gene transfer constrains the timing of methanogen evolution. Nature Ecology & Evolution. 2018;2(5):897-903.
2. Sorokin DY, Makarova KS, Abbas B, Ferrer M, Golyshin PN, Galinski EA, et al. Discovery of extremely halophilic, methyl-reducing euryarchaea provides insights into the evolutionary origin of methanogenesis. Nature Microbiology. 2017;2(8):1-11.
3. Martin WF, Sousa FL. Early microbial evolution: the age of anaerobes. Cold Spring Harbor Perspectives in Biology. 2016;8(2):a018127.
4. Sauterey B, Charnay B, Affholder A, Mazevet S, Ferrière R. Co-evolution of primitive methane-cycling ecosystems and early Earth's atmosphere and climate. Nature Communications. 2020;11(1):2705.
5. Ueno Y, Yamada K, Yoshida N, Maruyama S, Isozaki Y. Evidence from fluid inclusions for microbial methanogenesis in the early Archaean era. Nature. 2006;440(7083):516-9.
6. Spang A, Ettema TJG. Archaeal evolution: the methanogenic roots of Archaea. Nature Microbiology. 2017;2(8):1-2.
7. Adam PS, Kolyfetis GE, Bornemann TLV, Vorgias CE, Probst AJ. Genomic remnants of ancestral methanogenesis and hydrogenotrophy in Archaea drive anaerobic carbon cycling. Science Advances. 2022;8(44):eabm9651.
8. Wang Y, Wegener G, Williams TA, Xie R, Hou J, Tian C, et al. A methylotrophic origin of methanogenesis and early divergence of anaerobic multicarbon alkane metabolism. Science Advances. 2021;7(27):eabj1453.
9. Hinrichs K-U. Microbial fixation of methane carbon at 2.7 Ga: Was an anaerobic mechanism possible? Geochemistry, Geophysics, Geosystems. 2002;3(7):1-10.
10. Saunois M, Stavert AR, Poulter B, Bousquet P, Canadell JG, Jackson RB, et al. The Global Methane Budget 2000–2017. Earth System Science Data. 2020;12(3):1561-623.
11. Rosentreter JA, Borges AV, Deemer BR, Holgerson MA, Liu S, Song C, et al. Half of global methane emissions come from highly variable aquatic ecosystem sources. Nature Geoscience. 2021;14(4):225-30.
12. Garcia PS, Gribaldo S, Borrel G. Diversity and evolution of methane-related pathways in archaea. Annual Review of Microbiology. 2022;76:727-55.
13. Ferry JG, Kastead KA. Methanogenesis. Archaea: Molecular and Cellular Biology. 2007. p. 288-314.
14. Conrad R. The global methane cycle: recent advances in understanding the microbial processes involved. Environmental Microbiology Reports. 2009;1(5):285-92.

522 15. Scheller S, Goenrich M, Boecher R, Thauer RK, Jaun B. The key nickel enzyme of methanogenesis
523 catalyses the anaerobic oxidation of methane. Nature. 2010;465(7298):606-8.
524 16. Thauer RK. Methyl (alkyl)-coenzyme M reductases: nickel F-430-containing enzymes involved in
525 anaerobic methane formation and in anaerobic oxidation of methane or of short chain alkanes.
526 Biochemistry. 2019;58(52):5198-220.
527 17. Evans PN, Boyd JA, Leu AO, Woodcroft BJ, Parks DH, Hugenholtz P, et al. An evolving view of
528 methane metabolism in the Archaea. Nature Reviews Microbiology. 2019;17(4):219-32.
529 18. Thauer RK, Kaster AK, Seedorf H, Buckel W, Hedderich R. Methanogenic archaea: ecologically
530 relevant differences in energy conservation. Nature Reviews Microbiology. 2008;6(8):579-91.
531 19. Baker BJ, De Anda V, Seitz KW, Dombrowski N, Santoro AE, Lloyd KG. Diversity, ecology and
532 evolution of Archaea. Nature Microbiology. 2020;5(7):887-900.
533 20. Bueno de Mesquita CP, Wu D, Tringe SG. Methyl-based methanogenesis: an ecological and genomic
534 review. Microbiology and Molecular Biology Reviews. 2023;87(1):e00024-22.
535 21. Söllinger A, Urich T. Methylotrophic methanogens everywhere — physiology and ecology of novel
536 players in global methane cycling. Biochemical Society Transactions. 2019;47(6):1895-907.
537 22. Nobu MK, Narihiro T, Kuroda K, Mei R, Liu WT. Chasing the elusive Euryarchaeota class WSA2:
538 genomes reveal a uniquely fastidious methyl-reducing methanogen. The ISME Journal.
539 2016;10(10):2478-87.
540 23. Vanwonterghem I, Evans PN, Parks DH, Jensen PD, Woodcroft BJ, Hugenholtz P, et al.
541 Methylotrophic methanogenesis discovered in the archaeal phylum Verstraetearchaeota. Nature
542 Microbiology. 2016;1(12):1-9.
543 24. McKay LJ, Dlakic M, Fields MW, Delmont TO, Eren AM, Jay ZJ, et al. Co-occurring genomic
544 capacity for anaerobic methane and dissimilatory sulfur metabolisms discovered in the Korarchaeota.
545 Nature Microbiology. 2019;4(4):614-22.
546 25. Wang Y, Wegener G, Hou J, Wang F, Xiao X. Expanding anaerobic alkane metabolism in the domain
547 of Archaea. Nature Microbiology. 2019;4(4):595-602.
548 26. Evans PN, Parks DH, Chadwick GL, Robbins SJ, Orphan VJ, Golding SD, et al. Methane metabolism
549 in the archaeal phylum Bathyarchaeota revealed by genome-centric metagenomics. Science.
550 2015;350(6259):434-8.
551 27. Berghuis BA, Yu FB, Schulz F, Blainey PC, Woyke T, Quake SR. Hydrogenotrophic methanogenesis
552 in archaeal phylum Verstraetearchaeota reveals the shared ancestry of all methanogens. Proceedings
553 of the National Academy of Sciences. 2019;116(11):5037-44.
554 28. Liu YF, Chen J, Zaramela LS, Wang LY, Mbadinga SM, Hou ZW, et al. Genomic and transcriptomic
555 evidence supports methane metabolism in Archaeoglobi. mSystems. 2020;5(2):e00651-19.

29. Stetter KO, Lauerer G, Thomm M, Neuner A. Isolation of extremely thermophilic sulfate reducers: evidence for a novel branch of archaebacteria. Science. 1987;236(4803):822-4.
30. Slobodkina G, Allioux M, Merkel A, Cambon-Bonavita MA, Alain K, Jebbar M, et al. Physiological and genomic characterization of a hyperthermophilic archaeon *Archaeoglobus neptunius* sp. nov. isolated from a deep-sea hydrothermal vent warrants the reclassification of the genus *Archaeoglobus*. Frontiers in Microbiology. 2021;12:679245.
31. Boyd JA, Jungbluth SP, Leu AO, Evans PN, Woodcroft BJ, Chadwick GL, et al. Divergent methyl-coenzyme M reductase genes in a deep-subseafloor Archaeoglobi. The ISME Journal. 2019;13(5):1269-79.
32. Hua ZS, Wang YL, Evans PN, Qu YN, Goh KM, Rao YZ, et al. Insights into the ecological roles and evolution of methyl-coenzyme M reductase-containing hot spring Archaea. Nature Communications. 2019;10(1):4574.
33. Lynes MM, Krukenberg V, Jay ZJ, Kohtz AJ, Gobrogge CA, Spietz RL, et al. Diversity and function of methyl-coenzyme M reductase-encoding archaea in Yellowstone hot springs revealed by metagenomics and mesocosm experiments. ISME Communications. 2023;3(1):22.
34. Wang J, Qu Y-N, Evans PN, Guo Q, Zhou F, Nie M, et al. Evidence for nontraditional *mcr*-containing archaea contributing to biological methanogenesis in geothermal springs. Science Advances. 2023;9(26):eadg6004.
35. Buessecker S, Chadwick GL, Quan ME, Hedlund BP, Dodsworth JA, Dekas AE. Mcr-dependent methanogenesis in Archaeoglobaceae enriched from a terrestrial hot spring. The ISME Journal. 2023;17(10):1649-59.
36. Laso-Perez R, Krukenberg V, Musat F, Wegener G. Establishing anaerobic hydrocarbon-degrading enrichment cultures of microorganisms under strictly anoxic conditions. Nature Protocols. 2018;13(6):1310-30.
37. Brandis A, Thauer RK. Growth of *Desulfovibrio* species on hydrogen and sulphate as sole energy source. Microbiology. 1981;126(1):249-52.
38. Ai G, Zhu J, Dong X, Sun T. Simultaneous characterization of methane and carbon dioxide produced by cultured methanogens using gas chromatography/isotope ratio mass spectrometry and gas chromatography/mass spectrometry. Rapid Communications in Mass Spectrometry. 2013;27(17):1935-44.
39. Bushnell B. BBMap: a fast, accurate, splice-aware aligner. Lawrence Berkeley National Lab (LBNL), Berkeley, CA (United States); 2014 Mar 17.
40. Seemann T. Prokka: rapid prokaryotic genome annotation. Bioinformatics. 2014;30(14):2068-9.

589 41. Wu Y-W, Tang Y-H, Tringe SG, Simmons BA, Singer SW. MaxBin: an automated binning method
590 to recover individual genomes from metagenomes using an expectation-maximization algorithm.
591 Microbiome. 2014;2:26.
592 42. Kang DD, Froula J, Egan R, Wang Z. MetaBAT, an efficient tool for accurately reconstructing single
593 genomes from complex microbial communities. PeerJ. 2015;3:e1165.
594 43. Alneberg J, Bjarnason BS, de Bruijn I, Schirmer M, Quick J, Ijaz UZ, et al. Binning metagenomic
595 contigs by coverage and composition. Nature Methods. 2014;11(11):1144-6.
596 44. Miller IJ, Rees ER, Ross J, Miller I, Baxa J, Lopera J, et al. Autometa: automated extraction of
597 microbial genomes from individual shotgun metagenomes. Nucleic Acids Research. 2019;47(10):e57-
598 e.
599 45. Sieber CMK, Probst AJ, Sharrar A, Thomas BC, Hess M, Tringe SG, et al. Recovery of genomes from
600 metagenomes via a dereplication, aggregation and scoring strategy. Nature Microbiology.
601 2018;3(7):836-43.
602 46. Kohtz AJ, Jay ZJ, Lynes MM, Krukenberg V, Hatzenpichler R. Culexarchaeia, a novel archaeal class
603 of anaerobic generalists inhabiting geothermal environments. ISME Communications. 2022;2(1):86.
604 47. Parks DH, Imelfort M, Skennerton CT, Hugenholtz P, Tyson GW. CheckM: assessing the quality of
605 microbial genomes recovered from isolates, single cells, and metagenomes. Genome Research.
606 2015;25(7):1043-55.
607 48. Andrews S, Krueger F, Seconds-Pichon A, Biggins F, Wingett S. FastQC: A quality control tool for
608 high throughput sequence data. Babraham Bioinformatics: Babraham Institute; 2015.
609 49. Deng Z-L, Münch PC, Mreches R, McHardy AC. Rapid and accurate identification of ribosomal RNA
610 sequences via deep learning. Nucleic Acids Research. 2022;50(10):e60-e.
611 50. Stahl DA. Development and application of nucleic acid probes in bacterial systematics. Sequencing
612 and hybridization techniques in bacterial systematics. 1991:205-48.
613 51. Stetter KO. *Archaeoglobus fulgidus* gen. nov., sp. nov.: a new taxon of extremely thermophilic
614 archaebacteria. Systematic and Applied Microbiology. 1988;10:172-3.
615 52. Huber H, Jannasch H, Rachel R, Fuchs T, Stetter KO. *Archaeoglobus veneficus* sp. nov., a novel
616 facultative chemolithoautotrophic hyperthermophilic sulfite reducer, isolated from abyssal black
617 smokers. Systematic and Applied Microbiology. 1997;20(3):374-80.
618 53. Mori K, Maruyama A, Urabe T, Suzuki K-i, Hanada S. *Archaeoglobus infectus* sp. nov., a novel
619 thermophilic, chemolithoheterotrophic archaeon isolated from a deep-sea rock collected at Suiyo
620 Seamount, Izu-Bonin Arc, western Pacific Ocean. International Journal of Systematic and
621 Evolutionary Microbiology. 2008;58(4):810-6.

622 54. Watkins AJ, Roussel EG, Webster G, Parkes RJ, Sass H. Choline and N,N-dimethylethanolamine as
623 direct substrates for methanogens. Applied and Environmental Microbiology. 2012;78(23):8298-303.
624 55. Hocking WP, Stokke R, Roalkvam I, Steen IH. Identification of key components in the energy
625 metabolism of the hyperthermophilic sulfate-reducing archaeon *Archaeoglobus fulgidus* by
626 transcriptome analyses. Frontiers in Microbiology. 2014;5:95.
627 56. Li G, Rabe KS, Nielsen J, Engqvist MK. Machine learning applied to predicting microorganism
628 growth temperatures and enzyme catalytic optima. ACS Synthetic Biology. 2019;8(6):1411-20.
629 57. Mahapatra A, Patel A, Soares JA, Larue RC, Zhang JK, Metcalf WW, et al. Characterization of a
630 *Methanosarcina acetivorans* mutant unable to translate UAG as pyrrolysine. Molecular Microbiology.
631 2006;59(1):56-66.
632 58. Ferguson T, Soares JA, Lienard T, Gottschalk G, Krzycki JA. RamA, a protein required for reductive
633 activation of corrinoid-dependent methylamine methyltransferase reactions in methanogenic archaea.
634 Journal of Biological Chemistry. 2009;284(4):2285-95.
635 59. Estelmann S, Ramos-Vera WH, Gad'on N, Huber H, Berg IA, Fuchs G. Carbon dioxide fixation in
636 '*Archaeoglobus lithotrophicus*': are there multiple autotrophic pathways? FEMS Microbiology
637 Letters. 2011;319(1):65-72.
638 60. Ferry JG. How to make a living by exhaling methane. Annual Review of Microbiology. 2010;64:453-
639 73.
640 61. Chernyh NA, Neukirchen S, Frolov EN, Sousa FL, Miroshnichenko ML, Merkel AY, et al.
641 Dissimilatory sulfate reduction in the archaeon '*Candidatus* Vulcanisaeta moutnovskia' sheds light on
642 the evolution of sulfur metabolism. Nature Microbiology. 2020;5(11):1428-38.
643 62. Neukirchen S, Sousa FL. DiSCo: a sequence-based type-specific predictor of Dsr-dependent
644 dissimilatory sulphur metabolism in microbial data. Microbial Genomics. 2021;7(7).
645 63. Ramos AR, Keller KL, Wall JD, Pereira IAC. The membrane QmoABC complex interacts directly
646 with the dissimilatory adenosine 5′-phosphosulfate reductase in sulfate reducing bacteria. Frontiers in
647 Microbiology. 2012;3:137.
648 64. Adams MWW. The metabolism of hydrogen by extremely thermophilic, sulfur-dependent bacteria.
649 FEMS Microbiology Reviews. 1990;6(2-3):219-37.
650 65. Ma K, Schicho RN, Kelly RM, Adams M. Hydrogenase of the hyperthermophile *Pyrococcus furiosus*
651 is an elemental sulfur reductase or sulfhydrogenase: evidence for a sulfur-reducing hydrogenase
652 ancestor. Proceedings of the National Academy of Sciences. 1993;90(11):5341-4.
653 66. Hocking WP, Roalkvam I, Magnussen C, Stokke R, Steen IH. Assessment of the carbon monoxide
654 metabolism of the hyperthermophilic sulfate-reducing archaeon *Archaeoglobus fulgidus* VC-16 by
655 comparative transcriptome analyses. Archaea. 2015;2015.

656 67. Welte C, Deppenmeier U. Membrane-bound electron transport in *Methanosaeta thermophila*. Journal
657 of Bacteriology. 2011;193(11):2868-70.
658 68. Pereira IA, Haveman SA, Voordouw G. Biochemical, genetic and genomic characterization of
659 anaerobic electron transport pathways in sulphate-reducing delta-proteobacteria. Sulphate-Reducing
660 Bacteria: Environmental and Engineered Systems (LL, B and WA, H, eds), Cambridge University
661 Press, Cambridge, UK. 2007.
662 69. Grein F, Pereira IA, Dahl C. Biochemical characterization of individual components of the
663 *Allochromatium vinosum* DsrMKJOP transmembrane complex aids understanding of complex
664 function in vivo. Journal of Bacteriology. 2010;192(24):6369-77.
665 70. Wu K, Zhou L, Tahon G, Liu L, Li J, Zhang J, et al. Isolation of a methyl-reducing methanogen outside
666 the Euryarchaeota. In revision (https://doi.org/10.21203/rs.3.rs-2501667/v1).
667 71. Kohtz A, Krukenberg V, Petrosian N, Jay Z, Pilhofer M, Hatzenpichler R. Cultivation and
668 visualization of a methanogen of the phylum Thermoproteota. In revision
669 (https://doi.org/10.21203/rs.3.rs-2500102/v1)
670 72. Spang A, Caceres EF, Ettema TJG. Genomic exploration of the diversity, ecology, and evolution of
671 the archaeal domain of life. Science. 2017;357(6351):eaaf3883.
672

673 **Figure legends**

674 **Fig. 1.** Community composition and methane production of the methanogenic enrichment culture
675 containing *Ca.* Methanoglobus hypatiae LCB24. *(A)* Relative abundance of 16S rRNA gene amplicons in
676 the initial sediment from hot spring LCB024, the slurry collected in November 2021, slurry material used
677 to initiate enrichments in February 2022, the initial enrichment, and five subsequent transfers (T1-T5) are
678 shown. For comparison, the estimated relative abundance of two metagenomic samples (T4-MG and SIT-
679 MG) is included. The metagenome recovered from a replicate from the stable isotope tracing experiment
680 incubated in the presence of deuterated methylamine (SIT-MG) revealed *Ca.* M. hypatiae grew to 92.8%
681 relative abundance during the experiment. The two most abundant ASVs across enrichment transfers are
682 shown with other taxa collapsed. Other methanogenic archaea were not identified in the initial enrichment
683 or in any subsequent transfers. Relative sequence abundance for all ASVs is reported in SI Appendix, Table
684 S1. *(B)* Headspace methane produced over long-term cultivation. The time between transfers decreased
685 while the average maximum concentration of methane increased over time. Culture 1A represents the initial
686 enrichment. A history of methane measurements can be found in SI Appendix, Table S2. *(C)* Visualization
687 of *Ca.* M. hypatiae cells at T6 labeled via CARD-FISH by the general archaea probe Arch915 (red). DAPI
688 staining of cells is in blue. *(D)* Cell morphologies in enrichment culture LCB24 at T7 as observed by
689 scanning electron microscopy.

690 **Fig. 2.** Phylogenetic affiliation of *Ca.* M. hypatiae LCB24. *(A)* Maximum-likelihood tree, inferred with
691 fasttree and WAG model (midpoint root), using a concatenated alignment of 33 conserved single copy
692 proteins (list provided in SI Appendix, Table S4). References are colored by the habitat or type from which
693 sequences had been recovered: hot springs in Yellowstone National Park (YNP), yellow; Great Boiling
694 Spring (GBS), green; hot springs in China, blue; isolates from marine hydrothermal vent systems, dark
695 blue. *(B)* Maximum-likelihood tree inferred with fasttree using 16S rRNA genes with length in base pairs
696 (bp). *(C)* ANI and AAI analysis of reference Archaeoglobales MAGs and genomes. Asterisks (*) indicate
697 MAGs containing *mcrA*, apart from the MAG of *Ca.* M. hydrogenotrophicum bin74 which encodes a *mcrA*
698 that is interrupted by a stop codon. AAI and ANI values are provided in SI Appendix, Fig. S1. *(D)*
699 Maximum-likelihood tree, inferred with IQtree2 and the LG+C60+F+G model, from the amino acid
700 alignment of McrA. Dashed lines indicate McrA/AcrA groups: (I) McrA from methanogens and ANME
701 (MCR-type), (II) McrA from TACK lineages (MCR-type), (III) McrA-like from proposed and
702 experimentally confirmed alkane oxidizing archaea (ACR-type). Insert shows MAGs closely related to *Ca.*
703 M. hypatiae LCB24.

704 **Fig. 3.** Conversion of stable isotope labeled monomethylamine to methane by culture LCB24. *(A)*
705 Production of $^{13}CH_4$ in cultures amended with $^{13}CH_3$-NH_2 vs. $^{12}CH_3$-NH_2 (6 replicates). *(B)* Production of
706 CD_3H in cultures amended with CD_3-NH_2 (6 replicates). *(C)* Production of $^{13}CO_2$ in cultures amended with
707 $^{13}CH_3$-NH_2 vs. $^{12}CH_3$-NH_2. For plots A and B, ten total replicates across treatments were sacrificed during
708 mid-exponential phase for metagenomic or metatranscriptomic sequencing indicated by red arrows. $^{13}CH_4$,
709 CD_3H, or $^{13}CO_2$ production for the replicate allowed to reach stationary phase is shown as a dashed line
710 through open diamond symbols. *(D)* Production of $^{12}CH_4$ in cultures amended with ^{12}C-monomethylamine
711 ($^{12}CH_3$-NH_2; 2 replicates). Cultures incubated without substrates (2 replicates) and those to which the
712 inhibitor BES was added on day 0 (3 replicates) did not produce $^{12}CH_4$ over the course of the experiment.
713 *(E)* Production of $^{12}CH_4$ in cultures amended with $^{12}CH_3$-NH_2 to which BES was added on day 33 of
714 incubation (black arrow; 3 replicates). The average production of $^{12}CH_4$ leveled off and ceased after the
715 introduction of BES, indicating methane generation by *Ca.* M. hypatiae is MCR-dependent. Error bars
716 indicate standard deviation of biological replicates when applicable. Measurements of $^{12}CH_4$, $^{13}CH_4$, CD_3H,
717 and $^{13}CO_2$ for all replicates and controls are reported in Dataset S2. $^{12}CH_4$ measurements for all controls
718 and replicates are shown in SI Appendix, Fig. S4 and Dataset S3. *(F)* $^{12}CH_4$ production and fraction of *Ca.*
719 M. hypatiae cells in biological replicates incubated with $^{13}CH_3$-NH_2. Relative abundance of cells was
720 determined at three time points (day 22, 32, 45) based on the fraction of *Ca.* M. hypatiae specific CARD-
721 FISH counts (orange) versus total counts of DAPI stained cells (blue). Error bars indicate the standard
722 deviation for four biological replicates on days 22 and 32.

723 **Fig. 4.** Temperature and substrate range of culture LCB24. *(A)* Methane production from MMA was
724 observed between 64-70 ˚C. *(B)* Substrate range. Methane production was observed for MMA, DMA,
725 TMA, and in media prepared without yeast extract. LAC, lactate; MeOH, methanol. Both experiments
726 performed in triplicate. All measurements can be found in Dataset S4.
727

728 **Fig. 5.** Transcriptional activity in *Ca.* M. hypatiae grown under methanogenic conditions (N_2 headspace,
729 10 mM MMA, and 0.01% yeast extract). Transcriptionally active proteins are shown in bold black font.
730 Proteins not encoded in the MAG are colored in white and denoted in bold red font. Average reads per
731 kilobase of transcript per million mapped reads (RPKM) values of six biological replicates are depicted.
732 RPKM values are represented by boxes or colored subunits close to each protein and are colored according
733 to their expression level with the RPKM value of the lowest expressed gene depicted, 37 RPKM. For
734 enzymes comprising multiple subunits, the beta-oxidation pathway, and the TCA cycle, an average RPKM
735 value representing the transcribed enzymes is used. *Ca.* M. hypatiae is transcriptionally active under
736 methanogenic conditions and encodes the ability to convert methyl-groups from mono-, di-, and

737 trimethylamine to methane. This ability is enabled by several copies of substrate-specific
738 methyltransferases and corrinoid proteins highlighted in the box to the bottom right. A complete list of
739 genes described in this figure, their transcription levels, and their abbreviations is provided in Dataset S5.

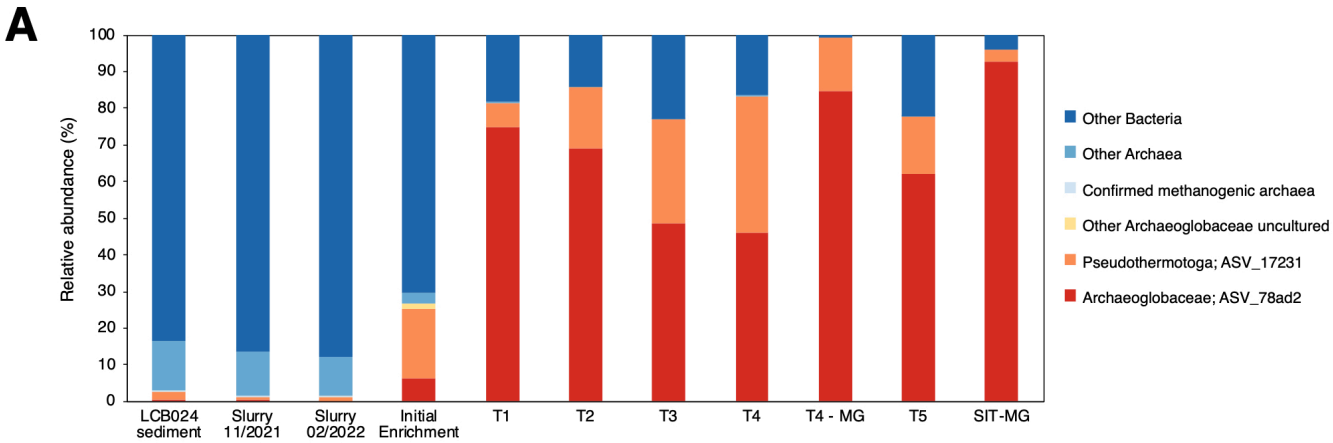
A
Relative abundance (%)
100
90
80
70
60
50
40
30
20
10
0
LCB024 sediment
Slurry 11/2021
Slurry 02/2022
Initial Enrichment
T1
T2
T3
T4
T4 - MG
T5
SIT-MG
Other Bacteria
Other Archaea
Confirmed methanogenic archaea
Other Archaeoglobaceae uncultured
Pseudothermotoga; ASV_17231
Archaeoglobaceae; ASV_78ad2

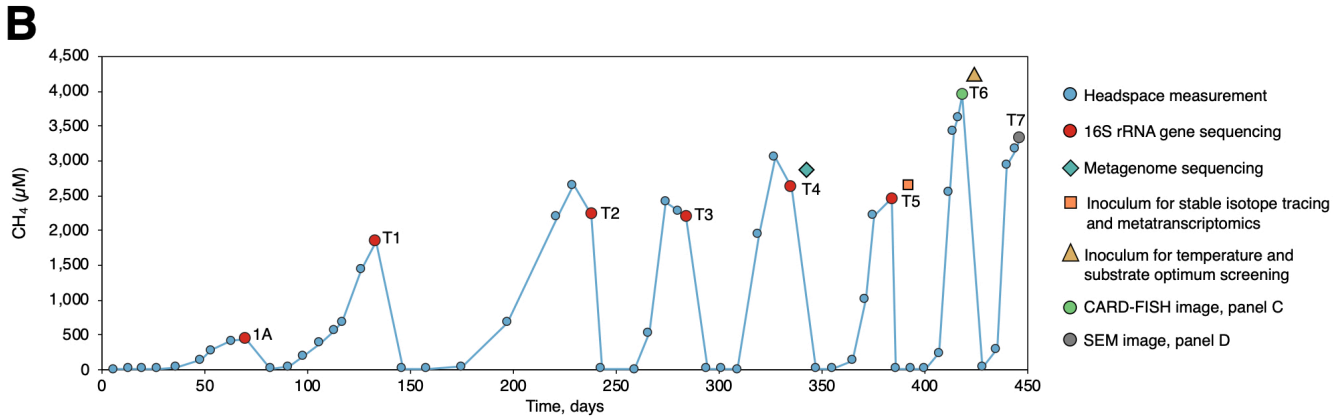
B
CH_4 (μM)
4,500
4,000
3,500
3,000
2,500
2,000
1,500
1,000
500
0
0
50
100
150
200
250
300
350
400
450
Time, days
1A
T1
T2
T3
T4
T5
T6
T7
Headspace measurement
16S rRNA gene sequencing
Metagenome sequencing
Inoculum for stable isotope tracing and metatranscriptomics
Inoculum for temperature and substrate optimum screening
CARD-FISH image, panel C
SEM image, panel D

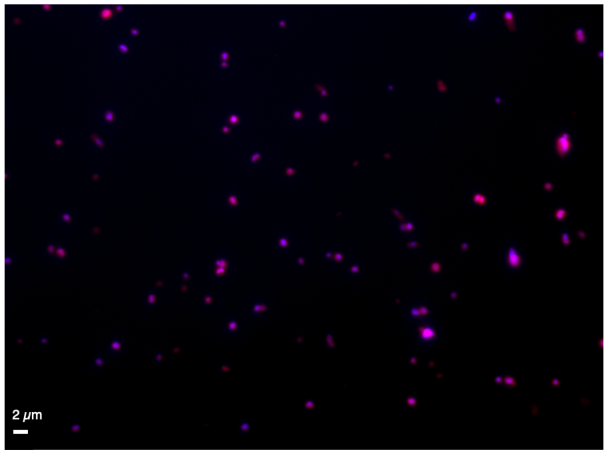
C
2 μm

D
2 μm

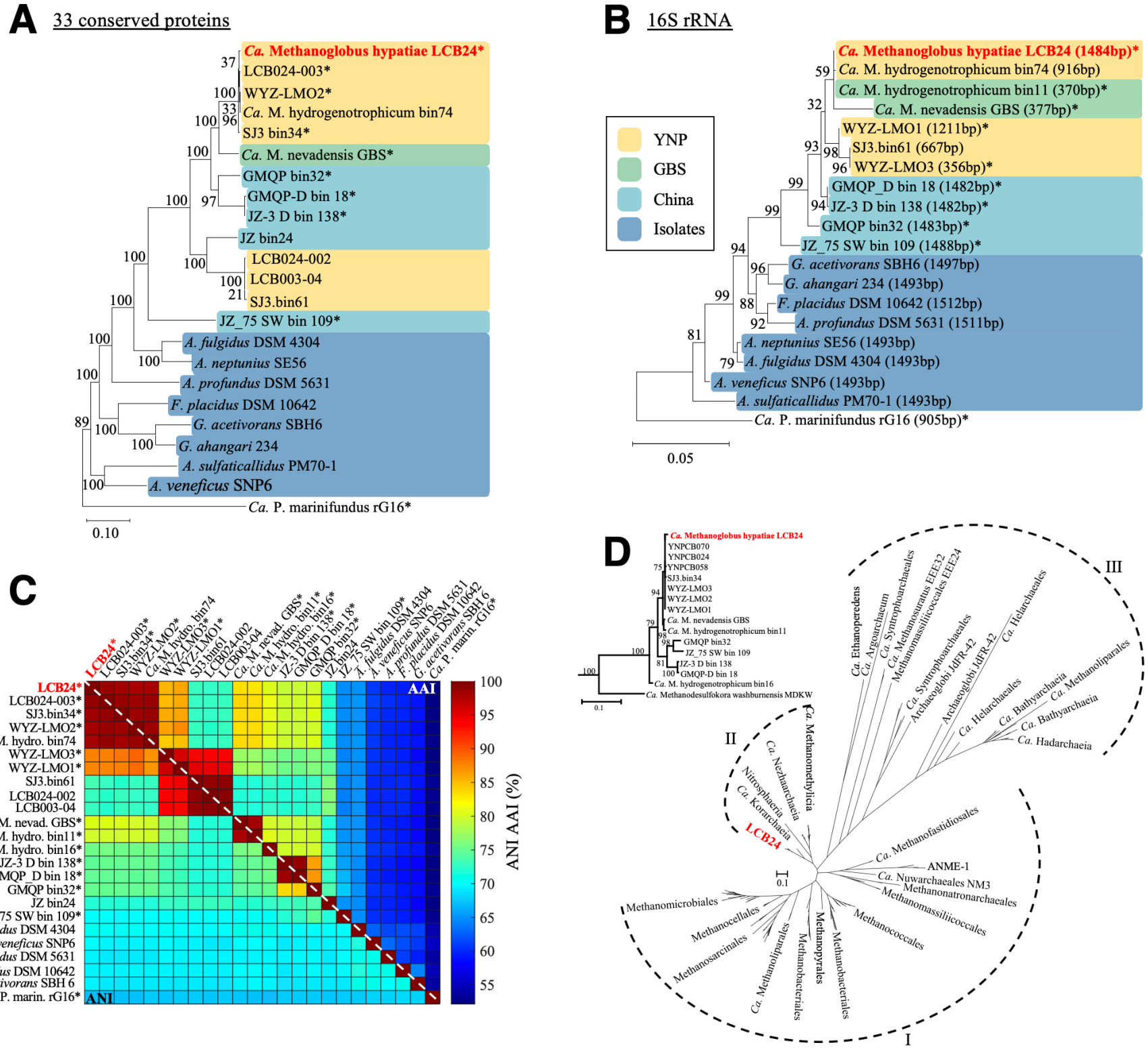
A
33 conserved proteins
Ca. Methanoglobus hypatiae LCB24*
LCB024-003*
WYZ-LMO2*
Ca. M. hydrogenotrophicum bin74
SJ3 bin34*
Ca. M. nevadensis GBS*
GMQP bin32*
GMQP-D bin 18*
JZ-3 D bin 138*
JZ bin24
LCB024-002
LCB003-04
SJ3.bin61
JZ_75 SW bin 109*
A. fulgidus DSM 4304
A. neptunius SE56
A. profundus DSM 5631
F. placidus DSM 10642
G. acetivorans SBH6
G. ahangari 234
A. sulfaticallidus PM70-1
A. veneficus SNP6
Ca. P. marinifundus rG16*
0.10
B
16S rRNA
YNP
GBS
China
Isolates
Ca. Methanoglobus hypatiae LCB24 (1484bp)*
Ca. M. hydrogenotrophicum bin74 (916bp)
Ca. M. hydrogenotrophicum bin11 (370bp)*
Ca. M. nevadensis GBS (377bp)*
WYZ-LMO1 (1211bp)*
SJ3.bin61 (667bp)
WYZ-LMO3 (356bp)*
GMQP_D bin 18 (1482bp)*
JZ-3 D bin 138 (1482bp)*
GMQP bin32 (1483bp)*
JZ_75 SW bin 109 (1488bp)*
G. acetivorans SBH6 (1497bp)
G. ahangari 234 (1493bp)
F. placidus DSM 10642 (1512bp)
A. profundus DSM 5631 (1511bp)
A. neptunius SE56 (1493bp)
A. fulgidus DSM 4304 (1493bp)
A. veneficus SNP6 (1493bp)
A. sulfaticallidus PM70-1 (1493bp)
Ca. P. marinifundus rG16 (905bp)*
0.05
C
LCB24*
LCB024-003*
SJ3.bin34*
WYZ-LMO2*
Ca. M. hydro. bin74
WYZ-LMO3*
WYZ-LMO1*
SJ3.bin61
LCB024-002
LCB003-04
Ca. M. nevad. GBS*
Ca. M. hydro. bin11*
Ca. M. hydro. bin16*
JZ-3 D bin 138*
GMQP_D bin 18*
GMQP bin32*
JZ bin24
JZ_75 SW bin 109*
A. fulgidus DSM 4304
A. veneficus SNP6
A. profundus DSM 5631
F. placidus DSM 10642
G. acetivorans SBH 6
Ca. P. marin. rG16*
AAI
ANI
ANI AAI (%)
D
Ca. Methanoglobus hypatiae LCB24
YNPCB070
YNPCB024
YNPCB058
SJ3.bin34
WYZ-LMO3
WYZ-LMO2
WYZ-LMO1
Ca. M. nevadensis GBS
Ca. M. hydrogenotrophicum bin11
GMQP bin32
JZ_75 SW bin 109
JZ-3 D bin 138
GMQP-D bin 18
Ca. M. hydrogenotrophicum bin16
Ca. Methanodesulfokora washburnensis MDKW
0.1
Ca. Ethanoperedens
Ca. Argoarchaeum
Ca. Syntrophoarchaeales
Ca. Methanosuratus EEE32
Methanomassiliicoccales EEE24
Ca. Syntrophoarchaeales
Archaeoglobi JdFR-42
Archaeoglobi JdFR-42
Ca. Helarchaeales
Ca. Helarchaeales
Ca. Bathyarchaeia
Ca. Methanoliparales
Ca. Bathyarchaeia
Ca. Hadarchaeia
III
II
Ca. Methanomethylicia
Ca. Nezhaarchaeia
Nitrosphaeria
Ca. Korarchaeia
LCB24
Ca. Methanofastidiosales
ANME-1
Ca. Nuwarchaeales NM3
Methanonatronarchaeales
Methanomassiliicoccales
Methanococcales
Methanobacteriales
Methanopyrales
Methanobacteriales
Ca. Methanoliparales
Methanosarcinales
Methanocellales
Methanomicrobiales
0.1
I

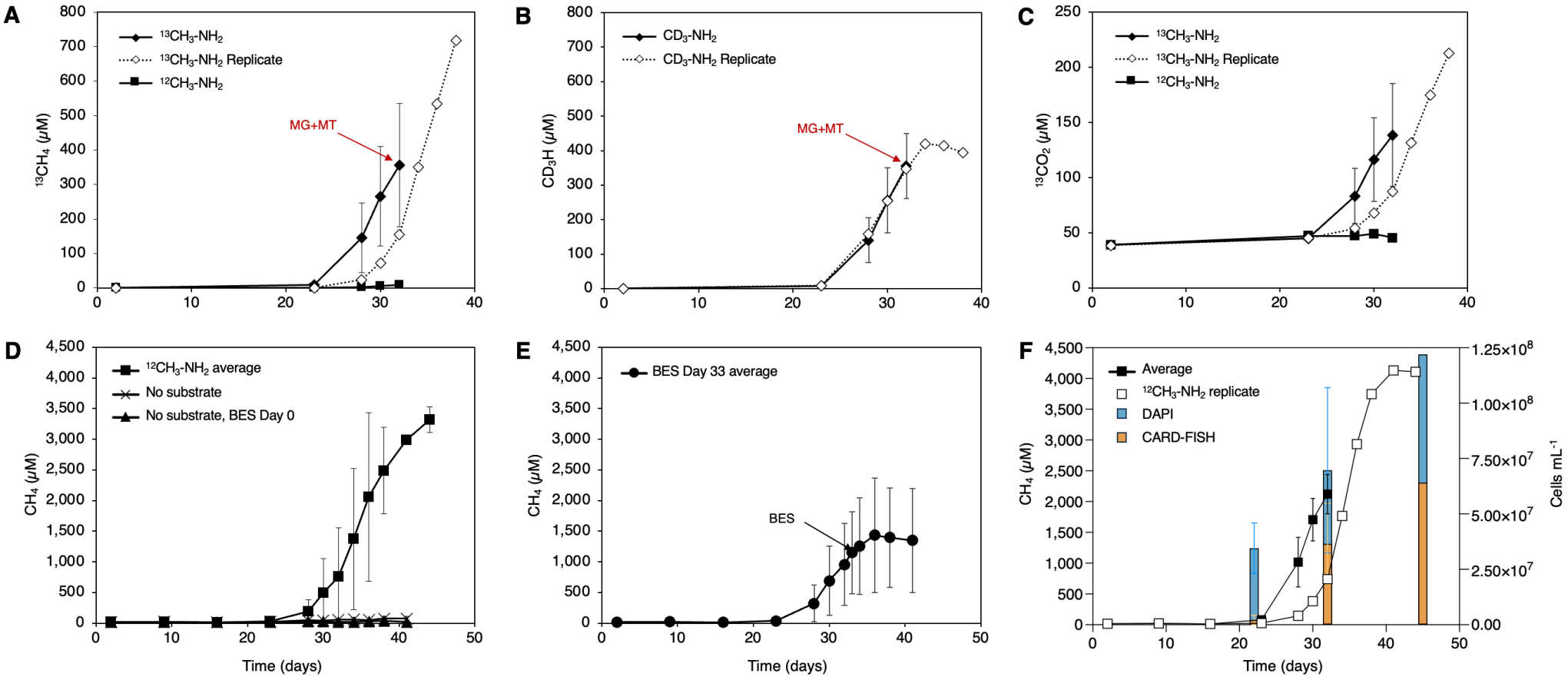
A
$^{13}CH_3$-NH_2
$^{13}CH_3$-NH_2 Replicate
$^{12}CH_3$-NH_2
MG+MT
$^{13}CH_4$ (μM)
B
CD_3-NH_2
CD_3-NH_2 Replicate
MG+MT
CD_3H (μM)
C
$^{13}CH_3$-NH_2
$^{13}CH_3$-NH_2 Replicate
$^{12}CH_3$-NH_2
$^{13}CO_2$ (μM)
D
$^{12}CH_3$-NH_2 average
No substrate
No substrate, BES Day 0
CH_4 (μM)
Time (days)
E
BES Day 33 average
BES
CH_4 (μM)
Time (days)
F
Average
$^{12}CH_3$-NH_2 replicate
DAPI
CARD-FISH
CH_4 (μM)
Cells mL^{-1}
Time (days)

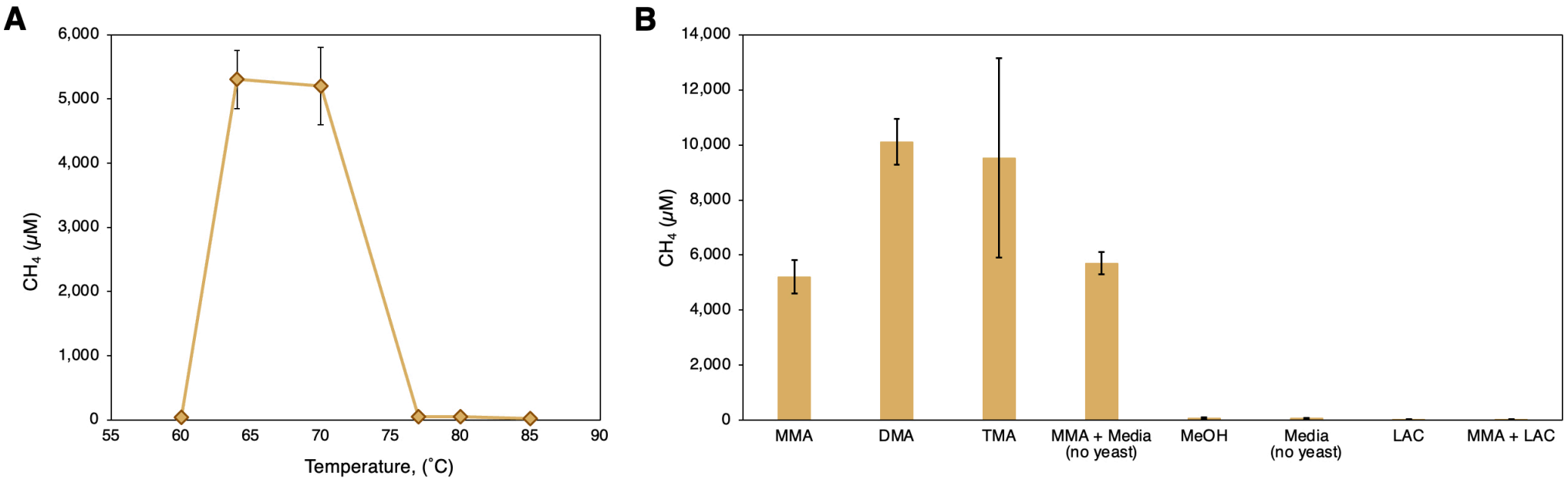
A
6,000
5,000
4,000
3,000
2,000
1,000
0
CH4 (μM)
55
60
65
70
75
80
85
90
Temperature, (˚C)
B
14,000
12,000
10,000
8,000
6,000
4,000
2,000
0
CH4 (μM)
MMA
DMA
TMA
MMA + Media (no yeast)
MeOH
Media (no yeast)
LAC
MMA + LAC

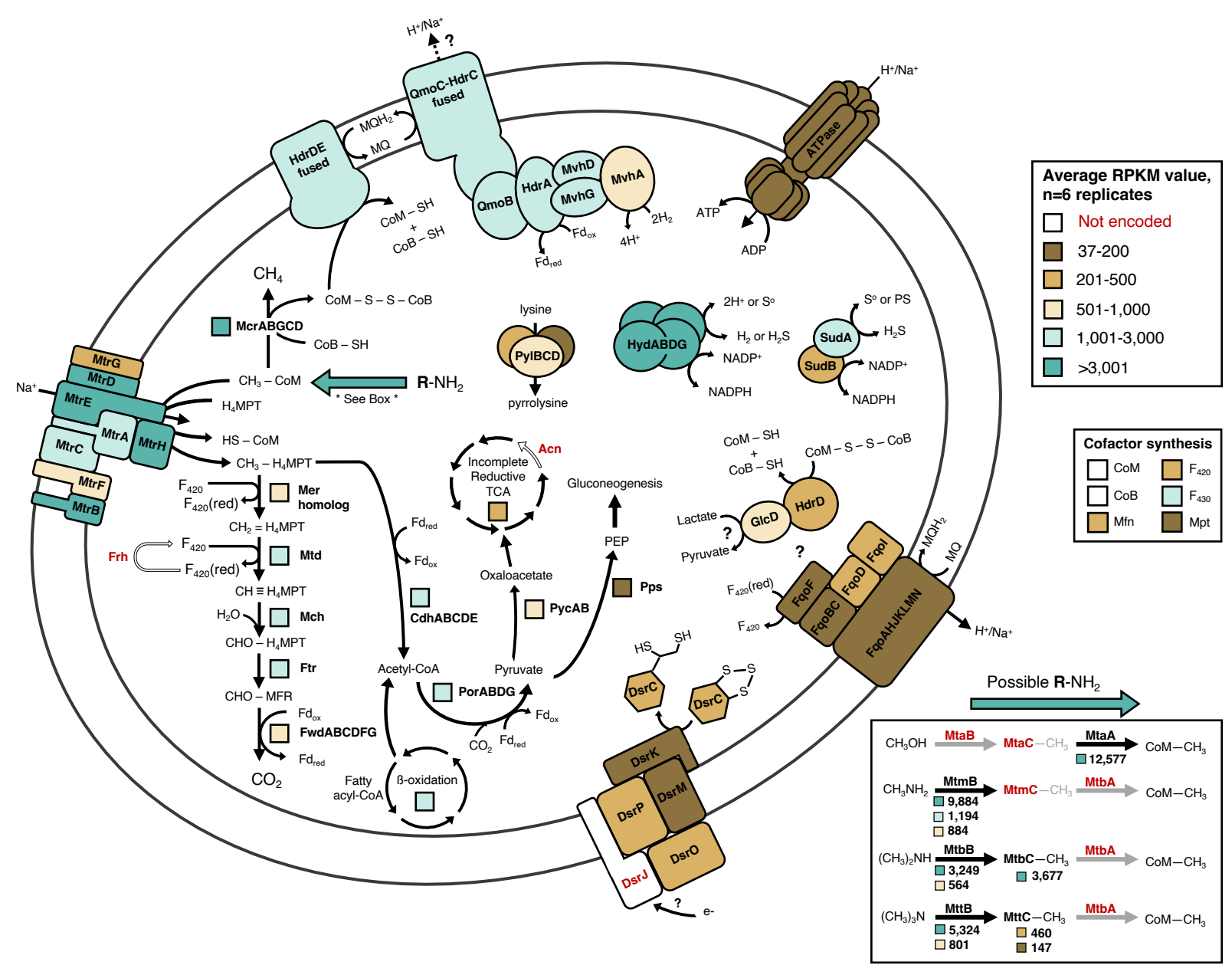
H+/Na+
?
QmoC-HdrC fused
HdrDE fused
MQH2
MQ
QmoB
HdrA
MvhD
MvhG
MvhA
2H2
4H+
Fdox
Fdred
ATPase
ATP
ADP
CoM – SH
+
CoB – SH
CH4
CoM – S – S – CoB
McrABGCD
CoB – SH
lysine
PylBCD
pyrrolysine
HydABDG
2H+ or S°
H2 or H2S
NADP+
NADPH
SudA
SudB
S° or PS
H2S
NADP+
NADPH
Average RPKM value, n=6 replicates
Not encoded
37-200
201-500
501-1,000
1,001-3,000
>3,001
Cofactor synthesis
CoM
CoB
Mfn
F420
F430
Mpt
MtrG
MtrD
MtrE
MtrA
MtrH
MtrC
MtrF
MtrB
Na+
CH3 – CoM
R-NH2
* See Box *
H4MPT
HS – CoM
CH3 – H4MPT
F420
F420(red)
Mer homolog
CH2 = H4MPT
Frh
Mtd
CH ≡ H4MPT
H2O
Mch
CHO – H4MPT
Ftr
CHO – MFR
FwdABCDFG
CO2
Acn
Incomplete Reductive TCA
Gluconeogenesis
Oxaloacetate
PycAB
Pps
PEP
CdhABCDE
Acetyl-CoA
Pyruvate
PorABDG
CO2
Fatty acyl-CoA
ß-oxidation
CoM – SH
+
CoB – SH
CoM – S – S – CoB
HdrD
GlcD
Lactate
Pyruvate
FqoF
FqoBC
FqoD
FqoI
FqoAHJKLMN
MQH2
MQ
H+/Na+
DsrC
DsrC
DsrK
DsrP
DsrM
DsrO
DsrJ
e-
Possible R-NH2
CH3OH
MtaB
MtaC—CH3
MtaA
12,577
CoM—CH3
CH3NH2
MtmB
9,884
1,194
884
MtmC—CH3
MtbA
CoM—CH3
(CH3)2NH
MtbB
3,249
564
MtbC—CH3
3,677
MtbA
CoM—CH3
(CH3)3N
MttB
5,324
801
MttC—CH3
460
147
MtbA
CoM—CH3

Supporting Information

SI Results and Discussion

Protologue

Methanoglobus hypatiae sp. nov.

Me.tha.no.glo.bus. Gr. pref. *methano*-, pertaining to methane; L. masc. n. -*globus*, sphere; Gr.L. masc. n. *Methanoglobus*, methane producing organism spherical in shape. This genus was named by Buessecker *et al.* (1). Hy.pa.ti.ae. Gr. fem. hypatiae, to honor Hypatia of Alexandria, a respected and renowned philosopher of ancient Alexandria, Egypt, who made significant contributions to the understanding of mathematics and astronomy. A symbol of intellectual courage and scholarly achievement. This archaeon was cultured from an unnamed hot spring in the Lower Culex Basin of Yellowstone National Park identified as feature LCB024 (2). This archaeon is an obligately anaerobic thermophile that performs methylotrophic methanogenesis using methylamines and grows as regular to irregular coccoid cells approximately 0.5 to 1 µm in width. The type genome of this archaeon is deposited at NCBI under BioProject PRJNA1014417, accession number will be added upon publication.

SI Materials and Methods

Amplicon Sequencing and Analysis

DNA was extracted from environmental slurry samples and enrichment cultures sampled on the day of transfer using the FastDNA Spin Kit for Soil (MP Biomedicals, Irvine, CA) following the manufacturer's guidelines. Archaeal and bacterial 16S rRNA genes were amplified with the updated Earth Microbiome Project primer set 515F and 806R (3). Amplicon libraries were prepared as previously described (2) and sequenced by the Molecular Research Core Facility at Idaho State University (Pocatello, ID) using an Illumina MiSeq platform with 2 x 250 bp paired end read chemistry. Gene reads were processed using QIIME 2 version 2022.8 (4). Primer sequences were removed from demultiplexed reads using cutadapt (5) with error rate 0.12 and reads truncated (130 bp forward, 150 bp reverse), filtered, denoised and merged in DADA2 with default settings (6). Processed 16S rRNA gene amplicon sequence variants (ASVs) were taxonomically classified with the sklearn method and the SILVA 138 database (7). The R package *decontam* (version 1.18.0) (8) was used to remove contaminants using the "Prevalence" model with a threshold of 0.5.

Annotation and Reconstruction of Metabolic Potential

Genes associated with methanogenesis pathways, dissimilatory sulfur metabolism pathways, coenzyme and cofactor biosynthesis, energy conservation, and beta-oxidation, were inventoried. Annotations assigned by Prokka were refined through manual evaluation using KofamKOALA, NCBI BLASTP, NCBI's Conserved Domain Database, InterPro, the hydrogenase classifier HydDB, and DiSCo (9-14).

Phylogenetic and Phylogenomic Analyses

Average nucleotide identities (ANI) of 16S rRNA genes were calculated with blastn, with ANI and average amino acid identities (AAI) calculated by pyani v02.2.12 (ANIb) and CompareM v0.0.23 (--fragLen 2000) (https://github.com/dparks1134/CompareM), respectively for selected Archaeoglobales genomes and MAGs (Table 1). Phylogenetic analysis of 16S rRNA genes was performed with fasttree (15) using masked alignments generated by ssu-align.

Archaeoglobales MAGs and reference genomes were screened for 54 phylogenetically informative single copy proteins (16, 17) of which a subset of 33 proteins were identified in them all (SI Appendix, Table S4). In order to maximize the number of proteins compared across references, MAGs LMO1 and LMO3 were excluded from this analysis, as they lacked 2 and 7 proteins out of the total 33, respectively. These were then aligned with muscle (18), concatenated, and phylogenomically analyzed with maximum likelihood analysis with fasttree (WAG model). McrA alignments were performed with MAFFT-LINSi v7.522 (19), trimmed with trimAL v1.4.rev22 (20) using a 0.5 gap threshold, and maximum likelihood trees were built with IQTree2 v2.0.6 (21) using LG+C60+F+G model and 1,000 ultrafast bootstraps.

Temperature and Substrate Optimum Experiments

Methane production and growth of Archaeoglobus was evaluated at different temperatures and in the presence of methylated substrates (i.e., methanol and mono-, di-, and trimethylamine), lactate, and media prepared without yeast extract. The sixth transfer of the enrichment was used to inoculate triplicate 30 mL serum bottles containing 15 mL of medium with 8% v/v inoculum, streptomycin (50 mg/L), vancomycin (50 mg/L), and 10 mM of each substrate tested. Cultures were evaluated at 60 ˚C, 64 ˚C, 70 ˚C, 77 ˚C, 80 ˚C, and 85 ˚C with 10 mM MMA. Separately, we tested whether the culture would grow on the following substrate (combinations): 10 mM dimethylamine (DMA); 10 mM trimethylamine (TMA); 10 mM methanol (MeOH); 10 mM lactate (LAC); 10 mM MMA and 10 mM LAC); 10 mM MMA with media without yeast extract; and a control in media without yeast or any methanogenic substrate. The 70 ˚C cultures amended with 10 mM MMA served as the control. All incubations were performed in biological triplicate.

Methane Measurements

During cultivation, 250 µL subsamples of the headspace were taken using a gas tight syringe (Hamilton) and injected into a 10 mL autosampler vial that had been sealed with grey chlorobutyl septa. Samples were taken from the autosampler vials and injected into a Shimadzu 2020-GC gas chromatograph equipped with a GS-CarbonPLOT column (30 m x 0.32 mm; 1.5 µm film thickness; Agilent) and a Rt-Q-BOND column (30 m x 0.32 mm; 1.5 µm film thickness; Restek) using helium as a carrier gas. All injections were performed by a Shimadzu AOC-6000 autosampler robot. The injector, column, and flame ionization detector (FID) were maintained at 200 ˚C, 50 ˚C, and 240 ˚C, respectively. Methane concentrations were calculated based on injection of a standard curve.

Fluorescence *in situ* hybridization and cell counts

Aliquots of enrichment cultures incubated with ^{13}C-MMA during the SIT experiment were treated with 2% paraformaldehyde (PFA) and fixed for 1 hr at room temperature. Following fixation, cells were washed twice with 1x PBS, followed by centrifugation at 16,000 × g to remove the supernatant, resuspended in 1x PBS, and stored at 4 ˚C. For direct cell counts, aliquots of fixed cell suspensions were filtered onto polycarbonate filters (0.2 µm pore size, 25 mm diameter, GTTP Millipore, Germany) and air dried before filter pieces were cut and embedded in 0.2% low melting agarose. We attempted to use the Archaeoglobales-specific probe Arglo32 (22), however fluorescent signal was insufficient. Given *Ca.* M. hypatiae was the sole archaeon in the enrichment culture, the relative abundance of *Ca.* M. hypatiae cells was determined via catalyzed reporter deposition fluorescence *in situ* hybridization (CARD-FISH) using the general archaea-targeted 16S rRNA oligonucleotide probe Arch915 (23). Total cell counts were based on DNA-stained cells using DAPI (4,6-diamidino-2-phenylindole). CARD-FISH was performed as previously described (24). Cell wall permeabilization was achieved with a brief treatment of 0.1 M HCl (1

89 min, RT) followed by treatment with 0.01 M HCl (15 min, RT). Endogenous peroxidases were inactivated
90 with 0.15% H_2O_2 in methanol (30 min, RT). A formamide concentration of 35% was used for all
91 hybridization reactions (2.5 hrs, 46˚C). CARD was performed using Alexa Fluor 594 labeled tyramides for
92 30 min at 46˚C. Following signal amplification, an additional washing step in 1x PBS was included to
93 reduce background fluorescence (15 min, RT, dark). Samples were stained with DAPI, embedded in
94 Citifluor-Vectashield, and enumerated using an epifluorescence microscope (Leica DM4B).
95
96 **Scanning electron microscopy (SEM)**
97 An aliquot of the enrichment culture at transfer 7 (T7) was treated with 2% paraformaldehyde (PFA) and
98 fixed for 1 hr at room temperature. Following fixation, cells were washed twice through centrifugation at
99 16,000 × g to remove the supernatant, resuspended in 1x phosphate buffered saline (PBS), and stored at 4
100 ˚C. Samples for imaging were prepared according to Schaible et al., 2022 (25). Briefly, a square coupon
101 of mirror-finished 304 stainless steel (25 mm diameter, 0.6 mm thickness) was purchased from Stainless
102 Supply (Monroe, NC). The coupon was cleaned by washing with a 1% solution of Tergazyme (Alconox,
103 New York, NY) and rinsed with Milli-Q water. The coupon was dried under compressed air and stored at
104 room temperature. 5 µL of fixed sample was spotted on the coupon and air-dried at 46 °C for 3 min. The
105 coupon was then dried for 1 m each step in a successive ethanol series starting with 10% ethanol and
106 increasing by increments of 10% with the last step 90% ethanol. SEM images were captured using a Zeiss
107 (Jena, Germany) SUPRA 55VP field emission scanning electron microscope (FE-SEM). The microscope
108 was operated at 1 keV under a vacuum of 0.2–0.3 mPa, with a working distance of 5.4-6.2 mm at the
109 Imagining and Chemical Analysis Laboratory (ICAL) of Montana State University (Bozeman, MT). No
110 conductivity coating was applied before SEM analysis as the microscope was operated at 1 keV.

SI Tables

Table S1. Extended community composition history of methanogenic enrichment cultures via estimated relative abundance (%) from 16S rRNA gene amplicon sequencing.

	LCB024 sediment	Slurry 11/2021	Slurry 02/2022	Initial Enrichment	T1	T2	T3	T4	T4 - MG	T5	SIT-MG
Archaeoglobaceae ASV_78ad2	0.46	0.32	0.02	6.42	74.8	68.9	48.5	46.0	84.7	62.2	92.8
Pseudothermotoga ASV_17231	2.14	1.06	1.08	18.93	6.8	17.1	28.5	37.4	14.5	15.7	3.2
Other Archaeoglobaceae uncultured	0.00	0.00	0.00	1.54	0.0	0.01	0.0	0.0	0.0	0.0	0.0
Confirmed methanogenic archaea	0.25	0.38	0.45	0.00	0.0	0.0	0.0	0.0	0.0	0.0	0.0
Other Archaea	13.51	11.87	10.49	2.67	0.0	0.0	0.0	0.04	0.0	0.0	0.0
Other Bacteria	83.63	86.37	87.95	70.44	18.4	14.1	23.1	16.5	0.8	22.1	4.0

Table S2. Methane production of the enrichment culture over time. T, transfer.

Culture ID	Days continuous	Days	CH_4 (μM)	CH_4 (mM)	CH_4 (ppm)	CH_4 (%)
1A – initial enrichment	6	6	4.91	0.00	118.67	0.01
	13	13	16.73	0.02	404.73	0.04
	20	20	12.98	0.01	314.13	0.03
	27	27	12.86	0.01	311.20	0.03
	36	36	32.92	0.03	796.48	0.08
	48	48	146.28	0.15	3538.80	0.35
	53	53	279.15	0.28	6753.17	0.68
	63	63	419.11	0.42	10139.33	1.01
	70	70	447.12	0.45	10816.36	1.08
T1	82	12	14.40	0.01	348.40	0.03
	91	21	50.85	0.05	1230.06	0.12
	98	27	198.41	0.20	4800.09	0.48
	106	35	390.47	0.39	9445.97	0.94
	113	42	565.32	0.57	13676.04	1.37
	117	46	688.44	0.69	16654.06	1.67
	126	55	1442.03	1.44	34885.74	3.49
	133	62	1844.13	1.84	44611.75	4.46
T2	146	7	15.22	0.02	368.32	0.04
	158	18	16.11	0.02	389.83	0.04
	175	34	49.40	0.05	1195.06	0.12
	197	57	680.54	0.68	16463.41	1.65
	221	81	2200.24	2.20	53227.90	5.32
	229	89	2654.34	2.65	64213.66	6.42
	238	98	2230.72	2.23	53964.66	5.40
T3	243	5	18.17	0.02	439.53	0.04
	259	21	10.70	0.01	258.82	0.03
	266	28	536.13	0.54	12969.71	1.30
	274	36	2413.23	2.41	58379.47	5.84
	280	42	2283.95	2.28	55253.34	5.53
	284	46	2193.96	2.19	53077.04	5.31
T4	294	10	17.36	0.02	420.07	0.04
	301	17	18.12	0.02	438.37	0.04
	309	25	12.51	0.01	302.54	0.03
	319	35	1944.01	1.94	47028.08	4.70
	327	43	3054.00	3.05	73881.94	7.39
	335	51	2619.45	2.62	63370.12	6.34
T5	347	10	13.41	0.01	324.42	0.03
	355	18	13.14	0.01	317.78	0.03
	365	28	137.59	0.14	3328.60	0.33
	371	34	1023.35	1.02	24756.27	2.48
	375	38	2218.75	2.22	53674.81	5.37
	384	46	2459.29	2.46	59493.85	5.95
T6	386	2	16.29	0.02	394.19	0.04
	393	9	21.33	0.02	516.14	0.05
	400	16	18.68	0.02	451.92	0.05
	407	23	245.86	0.25	5947.76	0.59
	412	28	2555.27	2.56	61815.61	6.18
	414	30	3432.93	3.43	83051.24	8.31
	416	32	3621.90	3.62	87623.79	8.76
	418	34	3942.97	3.94	95385.88	9.54
T7	428	9	34.33	0.03	830.38	0.08
	435	16	296.91	0.30	7182.55	0.72
	440	21	2931.05	2.93	70907.06	7.09
	444	25	3164.45	3.16	76553.52	7.66
	446	27	3338.04	3.34	80751.55	8.08

Table S3. Extended Archaeoglobales metagenome assembled genome and isolate genome statistics. A combined assembly of metagenomes from T4-MG and SIT-MG (Fig. 1A) for the *Ca.* M. hypatiae LCB24 MAG was used as it yielded an improved assembly. GTDB classified the YNP, GBS, and China MAGs as: d_Archaea;p_Halobacteriota;c_Archaeoglobi;o_Archaeoglobales; f_Archaeoglobaceae;g_WYZ-LMO2;s_WYZ-LMO2. Len., length; Compl., completeness; Redun, redundancy; Strain Hetero., strain heterogeneity; pOGT, predicted optimal growth temperature. [*] stop codon interrupts *mcrA* sequence; [a] Both sequences 5′ start; not identical; [b] Consists of 1 chromosome and 1 plasmid.

	Seqs	Len (Mb)	GC (%)	Compl. (%)	Redun. (%)	16S	tRNA	CDS	*mcrA*	CRISPRs	pOGT (°C)	Citation
***Ca.* M. hypatiae LCB24**	19	1.624	46.12	100	1.31	1	44	1,760	1	2	74.44	This study
Archaeoglobales LCB024-003	179	1.157	45.72	88.48	1.31	0	31	1,226	1	1	73.90	Lynes *et al.* 2023
Archaeoglobales WYZ-LMO2	220	1.514	45.92	97.60	0	0	40	1,614	1	2	72.40	Wang *et al.* 2019
Ca. M. hydrogenotrophicum bin74	127	1.547	45.63	92.81	1.31	1	34	1,679	0[*]	9	75.32	Liu *et al.* 2020
Archaeoglobales SJ3.Bin34	73	1.468	46.00	98.69	0.65	0	39	1,581	1	2	73.13	Colman *et al.* 2019
Ca. Methanoglobus nevadensis GBS	71	1.602	47.16	98.04	3.66	1	47	1,785	1	2	74.75	Peacock *et al.* 2013
Archaeoglobales GMQP bin32	20	1.727	41.26	100	0.98	1	39	1,931	1	2	71.88	Hua *et al.* 2019
Archaeoglobales GMQP_D bin 18	22	1.565	42.01	97.39	0.98	1	45	1,747	1	3	69.41	Wang *et al.* 2023
Archaeoglobales JZ-3 D bin 138	32	1.550	42.08	99.35	1.31	1	43	1,701	1	2	69.11	Wang *et al.* 2023
Archaeoglobales WYZ-LMO1	140	1.557	43.85	88.89	1.31	1	41	1,701	1	1	72.72	Wang *et al.* 2019
Archaeoglobales WYZ-LMO3	135	1.568	43.93	88.03	1.96	2[a]	35	1,670	1	2	73.09	Wang *et al.* 2019
Ca. M. hydrogenotrophicum bin11	252	1.220	47.59	91.83	6.17	1	27	1,387	1	0	72.64	Liu *et al.* 2020
Ca. M. hydrogenotrophicum bin16	46	1.668	45.49	96.51	1.31	0	41	1,864	1	2	72.69	Liu *et al.* 2020
Archaeoglobus JZ bin24	35	1.492	44.66	99.35	1.31	0	44	1,642	0	2	68.52	unpublished
Archaeoglobales LCB024-002	66	1.334	42.28	97.39	0.03	0	41	1,459	0	0	73.46	Lynes *et al.* 2023
Archaeoglobales LCB003-04	128	1.335	42.27	96.73	1.96	0	38	1,447	0	0	73.71	Lynes *et al.* 2023
Archaeoglobales SJ3.bin61	45	1.270	41.68	89.54	0	1	40	1,392	0	0	73.34	Colman *et al.* 2019
Archaeoglobales JZ_75 SW bin109	16	1.562	39.48	99.35	0.65	1	45	1,762	1	5	74.34	Wang *et al.* 2023
Archaeoglobus fulgidus DSM 4304	1	2.178	48.58	100	0	1	46	2,440	0	3	79.88	Klenk *et al.* 1997
Archaeoglobus neptunius SE56	32	2.116	46.05	100	0	1	47	2,336	0	2	78.26	Slobodkina *et al.* 2021
Archaeoglobus profundus DSM 5631	2[b]	1.563	46.05	100	0	1	48	1,784	0	0	85.86	von Jan *et al.* 2010
Ferroglobus placidus DSM 10642	1	2.196	44.14	100	0	1	49	2,467	0	1	83.83	Anderson *et al.* 2011
Geoglobus acetivorans SBH6	1	1.861	46.84	99.84	0	1	48	2,168	0	6	78.22	Mardanov *et al.* 2015
Geoglobus ahangari 234	1	1.770	53.11	100	0	1	46	1,985	0	7	84.11	Manzella *et al.* 2015
Archaeoglobus sulfaticallidus PM70-1	1	2.077	43.24	100	0	1	51	2,237	0	1	76.12	Stokke *et al.* 2013
Archaeoglobus veneficus SNP6	1	1.902	47.05	99.35	0	1	46	2,055	0	2	76.18	Mukherjee *et al.* 2017
Ca. Polytropus marinifundus rG16	21	2.129	40.22	99.84	1.96	1	44	2,286	2	0	66.39	Boyd *et al.* 2019

122 **Table S4.** Conserved single copy proteins used in phylogenomic analysis of MAGs and isolates.

arCOG	Gene	Product
arCOG00405	GRS1	Glycyl-tRNA synthetase (class II)
arCOG00779	RplO	Ribosomal protein L15
arCOG00785	RpmC	Ribosomal protein L29
arCOG01001	Map	Methionine aminopeptidase
arCOG01183	Kae1p/TsaD	Subunit of KEOPS complex, contains a domain with ASKHA fold and RIO-type kinase (AP-endonuclease activity)
arCOG01228	Ffh	Signal recognition particle GTPase
arCOG01722	RpsM/rps13p	Ribosomal protein S13
arCOG01758	RpsJ/rps10p	Ribosomal protein S10
arCOG04070	RplC	Ribosomal protein L3
arCOG04071	RplD	Ribosomal protein L4
arCOG04072	RplW	Ribosomal protein L23
arCOG04086	RpmD	Ribosomal protein L30
arCOG04087	RpsE	Ribosomal protein S5
arCOG04088	RplR	Ribosomal protein L18
arCOG04090	RplF/rpl6p	Ribosomal protein L6P
arCOG04091	RpsH/rps8p	Ribosomal protein S8
arCOG04094	RplX/rpl24p	Ribosomal protein L24
arCOG04095	RplN/rps14p	Ribosomal protein L14
arCOG04096	RpsQ/rps17p	Ribosomal protein S17
arCOG04097	RpsC/rps3p	Ribosomal protein S3
arCOG04098	RplV/rpl22p	Ribosomal protein L22
arCOG04113	RplP	Ribosomal protein L10AE/L16
arCOG04121	RnhB	Ribonuclease HII
arCOG04169	SecY	Preprotein translocase subunit SecY
arCOG04185	RpsO	Ribosomal protein S15P
arCOG04239	RpsD/rps4p	Ribosomal protein S4 or related protein
arCOG04242	RplM/rpl13p	Ribosomal protein L13
arCOG04243	RpsI/rps9p	Ribosomal protein S9
arCOG04245	RpsB/rps2p	Ribosomal protein S2
arCOG04255	RpsL/rps12p	Ribosomal protein S12
arCOG04256	RpoC/Rpo11	DNA-directed RNA polymerase subunit A"
arCOG04257	RpoC/Rpo3/rpoA1	DNA-directed RNA polymerase subunit A'
arCOG04277	Efp	Translation elongation factor P (EF-P)/translation initiation factor 5A (eIF-5A)

Table S5. Calculated cell density of replicates in the SIT experiment. FID measurements of replicates used to determine cell density. Density is calculated based on cell counts of DAPI and CARD-FISH labeled samples. Stdev., standard deviation. Letters A-F identify each replicate.

Summary	**$^{12}CH_4$**		**Cell Density, cells mL^{-1}**		
Replicate ID	**µM**	**ppm**	**DAPI**	**FISH**	**% labeled with Arch915**
5A Day 22	25	610	3.83×10^7	1.34×10^6	3.5
5B Day 22	57	1,374	1.88×10^7	5.07×10^6	12.7
5E Day 22	50	1,204	3.49×10^7	0	0
5F Day 22	132	3,196	4.59×10^7	2.21×10^6	4.8
Day 22 Average	66	1,596	3.45×10^7	2.16×10^6	5.3
Day 22 Stdev.	46	1,116	1.14×10^7	2.15×10^6	5.4
5A Day 32	741	17,917	4.26×10^7	2.85×10^7	66.9
5B Day 32	2,176	52,635	1.11×10^8	6.00×10^7	54.2
5E Day 32	1,779	43,035	3.40×10^7	1.74×10^7	51.2
5F Day 32	2,412	58,355	9.14×10^7	4.03×10^7	44.1
Day 32 Average	1,777	42,985	6.97×10^7	3.65×10^7	54.1
Day 32 Stdev.	739	17,868	3.73×10^7	1.82×10^7	9.6
5A Day 45	4,109	99,398	12.2×10^7	6.41×10^7	52.7

SI Figures

	LCB24	LCB024-003	SJ3-bin34	WYZ-LMO2	M. hydrogenotrophicum bin74	WYZ-LMO3	WYZ-LMO1	SJ3-bin61	LCB024-002	LCB003-04	M. nevadense GBS	M. hydrogenotrophicum bin11	M. hydrogenotrophicum bin16	JZ-3-D bin138	GMQP-D bin18	GMQPbin32	JZbin24	JZ-75-SW bin109	Afulgidus	Aneptunius	Aveneficus	Aprofundus	Asulfaticallidus	Fplacidus	Gacetivorans	Gahangari	P. marinifundus rG16
LCB24	100.0	98.6	98.1	97.8	97.8	85.3	86.0	73.0	72.5	72.9	83.3	83.2	80.5	79.2	79.3	79.8	71.9	64.8	65.0	64.4	60.6	59.7	58.9	59.6	58.9	58.9	52.5
LCB024-003	98.8	100.0	98.7	98.4	98.5	85.2	85.8	72.7	72.5	72.8	83.9	83.5	81.2	80.0	80.0	80.6	72.3	64.8	65.4	64.7	61.2	60.3	59.2	59.7	58.9	59.1	52.4
SJ3-bin34	98.5	98.9	100.0	98.3	98.5	85.7	86.0	72.6	72.5	72.9	83.5	83.5	81.0	79.6	79.8	80.2	71.9	64.9	65.1	64.7	60.7	59.9	59.1	59.7	58.9	59.0	52.5
WYZ-LMO2	98.2	98.6	98.4	100.0	98.4	86.3	87.1	73.0	72.2	72.7	83.4	83.6	80.7	79.5	79.3	79.7	71.6	64.6	64.9	64.4	60.6	59.7	58.9	59.5	58.9	58.9	52.6
M. hydrogenotrophicum bin74	98.0	98.7	98.3	98.6	100.0	84.4	84.8	72.8	72.4	72.8	83.4	83.4	80.8	79.8	79.7	80.3	72.1	64.8	65.3	64.6	60.7	59.7	58.9	59.5	59.0	58.9	52.6
WYZ-LMO3	87.9	87.9	88.2	89.1	87.1	100.0	95.9	94.2	94.0	94.2	77.2	77.0	76.2	75.3	75.4	76.2	74.9	64.5	65.0	64.5	60.5	59.9	59.1	59.5	58.5	58.7	52.2
WYZ-LMO1	87.5	87.6	87.7	88.9	86.7	96.3	100.0	95.0	94.6	94.8	77.5	77.8	76.3	75.4	75.4	76.0	74.9	65.0	64.8	64.3	60.5	60.1	59.1	59.7	58.9	58.7	52.4
SJ3-bin61	73.4	72.7	72.3	73.0	73.0	94.0	94.4	100.0	98.9	99.2	71.8	71.7	72.4	72.1	72.1	72.6	76.3	64.3	65.2	64.5	60.1	60.0	59.5	60.2	59.1	59.2	53.0
LCB024-002	73.1	72.3	72.7	72.5	72.6	94.0	94.3	98.7	100.0	99.4	71.8	71.5	72.3	71.9	72.0	72.6	76.3	64.1	65.1	64.3	60.1	60.1	59.3	59.9	58.8	58.9	52.9
LCB003-04	73.1	72.1	72.8	72.6	72.4	94.0	94.3	98.8	99.2	100.0	72.0	71.7	72.5	72.0	72.0	72.7	76.3	64.2	65.2	64.7	60.1	60.1	59.5	60.0	58.9	58.9	52.7
M. nevadense GBS	80.2	80.2	80.2	80.0	80.0	76.6	76.3	71.7	71.9	71.8	100.0	98.2	80.1	79.4	79.3	78.9	71.7	65.1	65.2	64.5	60.2	59.6	58.8	59.2	58.5	58.7	52.4
M. hydrogenotrophicum bin11	80.1	80.1	80.1	80.1	80.0	76.4	76.2	71.7	71.9	71.9	97.7	100.0	80.7	79.8	79.8	79.5	71.7	64.9	65.2	64.6	60.3	59.7	58.9	59.3	58.6	58.6	52.2
M. hydrogenotrophicum bin16	75.4	75.6	75.5	75.4	75.5	73.8	73.6	71.7	71.8	71.8	75.8	76.1	100.0	79.8	79.9	80.0	72.4	65.6	65.4	64.2	60.8	60.4	59.2	59.6	58.9	59.0	53.1
JZ-3-D bin138	74.8	75.0	74.9	74.8	75.0	73.5	73.2	71.8	71.8	71.8	74.6	74.9	75.2	100.0	98.7	86.3	72.5	65.7	64.7	63.8	60.0	59.5	58.5	58.8	58.2	58.4	52.5
GMQP-D bin18	74.8	74.9	74.9	74.8	75.0	73.4	73.2	71.7	71.7	71.7	74.6	74.8	75.2	98.4	100.0	86.6	72.7	66.7	64.7	63.8	60.0	59.4	58.6	58.8	58.4	58.4	52.5
GMQPbin32	75.0	75.1	74.9	74.9	75.1	73.7	73.4	72.0	72.0	72.0	74.4	74.5	75.0	83.7	84.1	100.0	73.7	67.8	64.9	64.0	60.6	60.1	59.0	59.2	58.7	58.7	53.0
JZbin24	71.9	71.9	71.8	71.8	71.8	72.6	72.6	72.9	72.9	73.0	72.0	72.2	72.4	73.0	73.2	73.7	100.0	65.0	64.8	64.1	60.0	59.8	59.2	59.2	58.3	58.8	52.5
JZ-75-SW bin109	70.1	70.0	70.0	70.0	70.1	70.4	70.3	70.2	70.2	70.2	70.2	70.4	70.4	71.9	72.7	74.6	71.7	100.0	64.8	63.8	60.4	60.0	58.9	59.6	58.9	58.8	52.8
Afulgidus	70.6	70.3	70.4	70.4	70.3	70.4	70.2	70.0	69.9	70.0	71.0	70.8	70.7	70.0	70.1	70.1	70.2	70.0	100.0	75.9	62.8	61.6	62.0	61.7	61.2	61.9	54.2
Aneptunius	70.2	70.1	70.1	70.0	70.0	70.3	70.0	70.0	69.9	70.0	70.4	70.3	69.9	69.8	69.8	70.0	69.7	70.0	74.2	100.0	62.3	61.0	61.3	60.6	60.5	60.8	53.6
Aveneficus	69.9	69.5	69.7	69.7	69.5	69.7	69.5	69.4	69.3	69.3	70.0	70.2	70.1	69.4	69.5	69.6	69.6	69.5	71.4	70.7	100.0	63.0	63.0	61.8	60.9	61.9	55.4
Aprofundus	69.6	69.2	69.3	69.1	69.3	69.9	69.7	69.6	69.5	69.5	69.5	69.7	69.5	69.6	69.8	69.9	69.3	70.1	70.8	70.3	70.7	100.0	60.0	61.1	59.6	60.0	53.7
Asulfaticallidus	70.0	69.4	69.7	69.5	69.7	69.7	69.5	69.6	69.3	69.4	69.7	70.1	69.4	69.5	69.8	69.8	69.1	69.8	71.5	70.8	71.3	70.6	100.0	60.2	60.2	61.0	54.1
Fplacidus	69.6	69.4	69.4	69.4	69.4	69.6	69.5	69.7	69.5	69.5	69.9	70.1	69.8	69.3	69.7	69.8	69.6	69.9	71.6	70.5	70.8	71.2	70.3	100.0	64.4	65.6	54.7
Gacetivorans	69.6	69.2	69.3	69.3	69.3	69.2	69.1	69.2	69.0	69.0	69.6	69.8	69.4	68.9	69.1	69.3	69.0	69.3	71.1	70.9	70.7	70.3	70.8	70.9	100.0	75.0	53.8
Gahangari	70.3	69.8	70.1	70.0	70.0	69.7	69.5	69.3	69.1	69.2	70.2	70.5	70.0	69.1	69.4	69.4	69.4	69.1	72.4	70.9	71.5	70.4	71.5	71.7	74.3	100.0	53.9
P. marinifundus rG16	67.3	67.3	67.3	67.2	67.5	67.4	67.6	67.6	67.5	67.5	67.3	67.2	67.1	67.7	67.6	67.6	67.5	67.8	67.7	68.1	68.1	68.2	68.2	68.3	68.2	67.3	100.0

Fig. S1. Detailed ANI (lower half of matrix) and AAI (upper half of matrix) analysis of related Archaeoglobales MAGs and reference genomes.

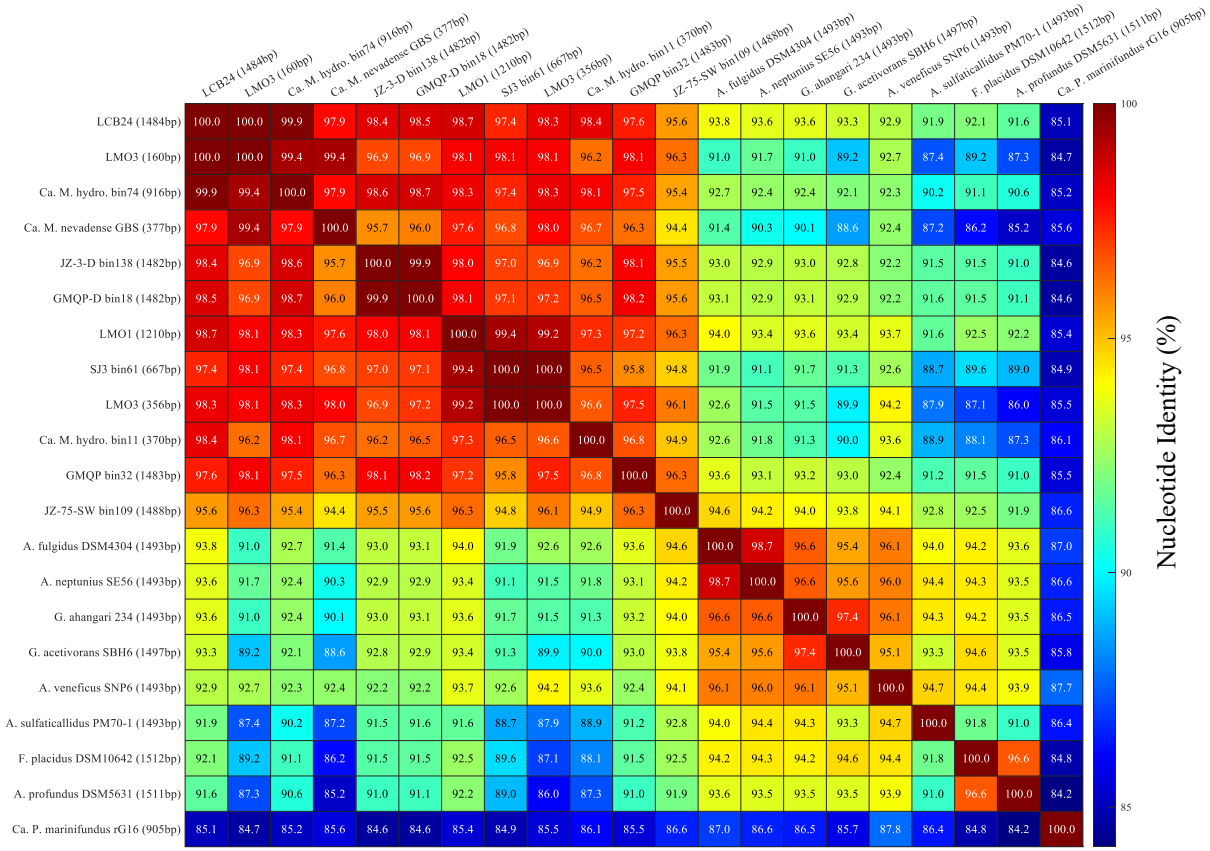

Fig. S2. 16S rRNA nucleotide identity analysis of closely related Archaeoglobales MAGs and reference genomes.

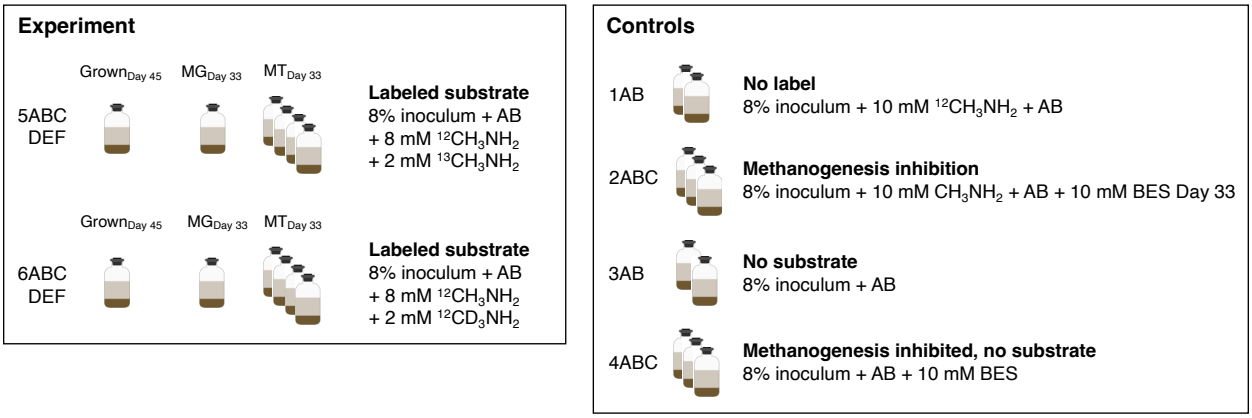

Fig. S3. Experimental setup of the stable isotope tracing (SIT) experiment. Incubations were carried out in 30 mL culture volumes in 60 mL serum bottles with 8% v/v inoculum, 50 mg/L streptomycin, 50 mg/L vancomycin, 10 mM MMA, and N_2 gas (99.999%) incubated in anoxic media (pH 7.8, 70 ˚C). Replicates sacrificed for analysis during mid-log phase are indicated. Of the eight samples harvested for metatranscriptomics, six were sequenced and used for analysis as two replicates did not yield sufficient RNA for sequencing. AB, antibiotics streptomycin and vancomycin, MG, metagenome sample; MT, metatranscriptome sample; BES, bromoethanesulfonate/methanogenesis inhibitor.

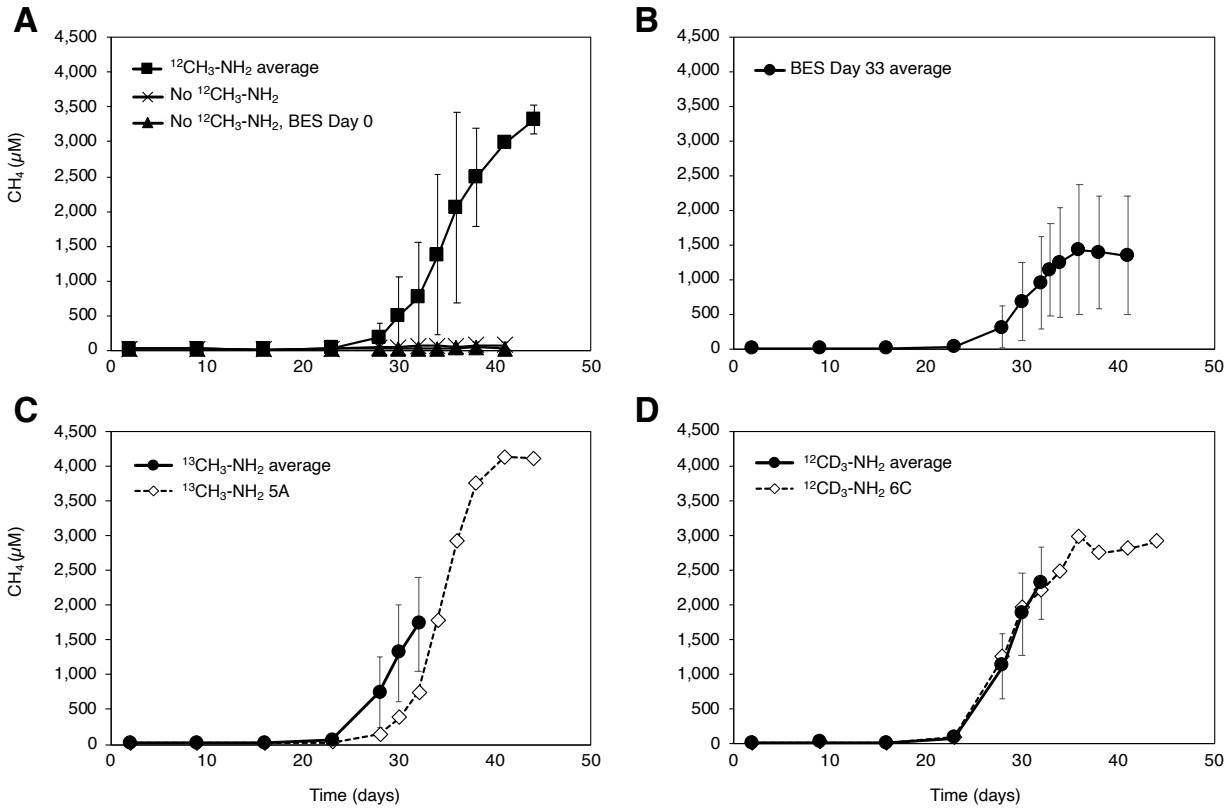

Fig. S4. $^{12}CH_4$ measurements by GC-FID during the stable isotope tracing experiment. Measurements can be found in Dataset S3.

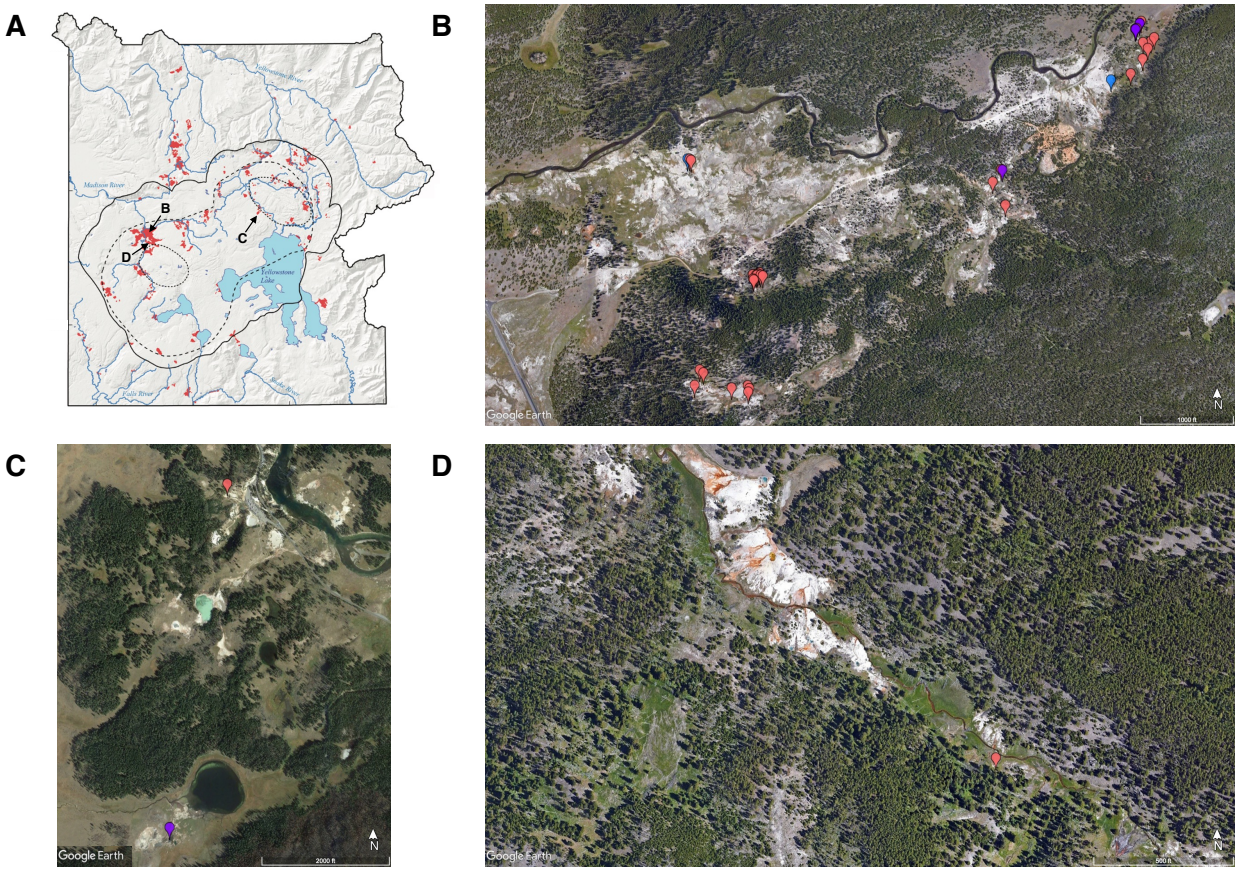

Fig. S5. Geographical distribution of geothermal features in Yellowstone National Park in which Archaeoglobi-related *mcrA* genes (n = 36) and *Ca.* M. hypatiae-related 16S rRNA genes (n = 6) were detected. Features are located in the (*A*) Map of Yellowstone National Park Wyoming, USA modified from Vaughan *et al.* 2014 (26) *(B)* Lower Culex Basin (n = 36), (*C*) Mud Volcano Region (n = 2), and (*D*) the White Creek Area (n = 1). These features spanned a wide pH (2.61-9.35) and temperature (18.4-93.8 ºC) range. Features in which *mcrA* were detected are marked in red and features with related 16S rRNA genes are shown in blue. Features in which both amplicons were detected are colored in purple. For details on these sites, their *mcrA* data, water geochemistry, and exact location, see Lynes & Krukenberg et al., 2023. Image source: Google Earth.

192 **Description of Available Supplementary Datasets**
193
194 **SI Dataset S1.** Extended metagenome assembled genome (SIT-MG) and isolate genome statistics. Seqs,
195 sequences; avg_cov, average coverage; avg_gc, average G+C content; % rel. abund., percent relative
196 abundance.
197
198 **SI Dataset S2.** GCMS measurements of masses 16 (CH_4), 17 ($^{13}CH_4$), and 19 ($^{12}CD_3H$) during the isotope
199 tracing experiment. Percent of labeled methane is calculated as a fraction of provided labeled substrate.
200 Stdev, standard deviation.
201
202 **SI Dataset S3.** Gas chromatograph FID measurements of $^{12}CH_4$ during isotope tracing experiment. NA,
203 not available/measured.
204
205 **SI Dataset S4.** Gas chromatograph FID measurements of CH_4 during temperature optimum experiment.
206 NA, not available/measured.
207
208 **SI Dataset S5.** Inventory of genes expressed by *Ca.* M. hypatiae LCB24 under methanogenic conditions
209 and as depicted in Fig. 5. Expression levels averaged across six replicates are reported in reads per kilobase
210 of transcript per million mapped reads (RPKM).
211
212 **SI Dataset S6.** Inventory of genes expressed by Ca. M. hypatiae LCB24 under methanogenic conditions
213 belonging to the beta-oxidation pathway. Expression levels averaged across six replicates are reported in
214 reads per kilobase of transcript per million mapped reads (RPKM).

References

1. Buessecker S, Chadwick GL, Quan ME, Hedlund BP, Dodsworth JA, Dekas AE. Mcr-dependent methanogenesis in Archaeoglobaceae enriched from a terrestrial hot spring. The ISME Journal. 2023;17(10):1649-59.
2. Lynes MM, Krukenberg V, Jay ZJ, Kohtz AJ, Gobrogge CA, Spietz RL, et al. Diversity and function of methyl-coenzyme M reductase-encoding archaea in Yellowstone hot springs revealed by metagenomics and mesocosm experiments. ISME Communications. 2023;3(1):22.
3. Apprill A, McNally S, Parsons R, Weber L. Minor revision to V4 region SSU rRNA 806R gene primer greatly increases detection of SAR11 bacterioplankton. Aquatic Microbial Ecology. 2015;75(2):129-37.
4. Bolyen E, Rideout JR, Dillon MR, Bokulich NA, Abnet CC, Al-Ghalith GA, et al. Reproducible, interactive, scalable and extensible microbiome data science using QIIME 2. Nature Biotechnology. 2019;37(8):852-7.
5. Martin M. Cutadapt removes adapter sequences from high-throughput sequencing reads. EMBnetjournal. 2011;17(1):10-2.
6. Callahan BJ, McMurdie PJ, Rosen MJ, Han AW, Johnson AJ, Holmes SP. DADA2: High-resolution sample inference from Illumina amplicon data. Nature Methods. 2016;13(7):581-3.
7. Quast C, Pruesse E, Yilmaz P, Gerken J, Schweer T, Yarza P, et al. The SILVA ribosomal RNA gene database project: improved data processing and web-based tools. Nucleic Acids Research. 2012;41(D1):D590-D6.
8. Davis NM, Proctor DM, Holmes SP, Relman DA, Callahan BJ. Simple statistical identification and removal of contaminant sequences in marker-gene and metagenomics data. Microbiome. 2018;6(1):226.
9. Aramaki T, Blanc-Mathieu R, Endo H, Ohkubo K, Kanehisa M, Goto S, et al. KofamKOALA: KEGG Ortholog assignment based on profile HMM and adaptive score threshold. Bioinformatics. 2020;36(7):2251-2.
10. Lu S, Wang J, Chitsaz F, Derbyshire MK, Geer RC, Gonzales NR, et al. CDD/SPARCLE: the conserved domain database in 2020. Nucleic Acids Research. 2020;48(D1):D265-D8.
11. Sondergaard D, Pedersen CN, Greening C. HydDB: A web tool for hydrogenase classification and analysis. Scientific Reports. 2016;6(1):34212.
12. Blum M, Chang H-Y, Chuguransky S, Grego T, Kandasaamy S, Mitchell A, et al. The InterPro protein families and domains database: 20 years on. Nucleic Acids Research. 2021;49(D1):D344-D54.
13. Neukirchen S, Sousa FL. DiSCo: a sequence-based type-specific predictor of Dsr-dependent dissimilatory sulphur metabolism in microbial data. Microb Genom. 2021;7(7).
14. Neukirchen S, Sousa FL. DiSCo: a sequence-based type-specific predictor of Dsr-dependent dissimilatory sulphur metabolism in microbial data. Microbial Genomics. 2021;7(7).
15. Price MN, Dehal PS, Arkin AP. FastTree 2--approximately maximum-likelihood trees for large alignments. PLoS One. 2010;5(3):e9490.
16. Jay ZJ, Beam JP, Dlakic M, Rusch DB, Kozubal MA, Inskeep WP. Marsarchaeota are an aerobic archaeal lineage abundant in geothermal iron oxide microbial mats. Nature Microbiology. 2018;3(6):732-40.
17. Zaremba-Niedzwiedzka K, Caceres EF, Saw JH, Backstrom D, Juzokaite L, Vancaester E, et al. Asgard archaea illuminate the origin of eukaryotic cellular complexity. Nature. 2017;541(7637):353-8.
18. Edgar RC. MUSCLE: multiple sequence alignment with high accuracy and high throughput. Nucleic Acids Research. 2004;32(5):1792-7.
19. Katoh K, Standley DM. MAFFT multiple sequence alignment software version 7: improvements in performance and usability. Molecular Biology and Evolution. 2013;30(4):772-80.
20. Capella-Gutiérrez S, Silla-Martínez JM, Gabaldón T. trimAl: a tool for automated alignment trimming in large-scale phylogenetic analyses. Bioinformatics. 2009;25(15):1972-3.
21. Minh BQ, Schmidt HA, Chernomor O, Schrempf D, Woodhams MD, von Haeseler A, et al. IQ-TREE 2: new models and efficient methods for phylogenetic inference in the genomic era. Molecular Biology and Evolution. 2020;37(5):1530-4.
22. Rusch A, Amend JP. Order-specific 16S rRNA-targeted oligonucleotide probes for (hyper) thermophilic archaea and bacteria. Extremophiles. 2004;8:357-66.

23. Stahl DA. Development and application of nucleic acid probes in bacterial systematics. Sequencing and hybridization techniques in bacterial systematics. 1991:205-48.
24. Pernthaler A, Pernthaler J, Amann R. Fluorescence in situ hybridization and catalyzed reporter deposition for the identification of marine bacteria. Applied and Environmental Microbiology. 2002;68(6):3094-101.
25. Schaible GA, Kohtz AJ, Cliff J, Hatzenpichler R. Correlative SIP-FISH-Raman-SEM-NanoSIMS links identity, morphology, biochemistry, and physiology of environmental microbes. ISME Communications. 2022;2(1):52.
26. Vaughan RG, Heasler HP, Jaworowski C, Lowenstern JB, Keszthelyi LP. Provisional maps of thermal areas in Yellowstone National Park based on satellite thermal infrared imaging and field observations: US Department of the Interior, US Geological Survey; 2014.
27. Wang Y, Wegener G, Hou J, Wang F, Xiao X. Expanding anaerobic alkane metabolism in the domain of Archaea. Nature Microbiology. 2019;4(4):595-602.
28. Liu YF, Chen J, Zaramela LS, Wang LY, Mbadinga SM, Hou ZW, et al. Genomic and transcriptomic evidence supports methane metabolism in Archaeoglobi. mSystems. 2020;5(2):e00651-19.
29. Colman DR, Lindsay MR, Amenabar MJ, Boyd ES. The intersection of geology, geochemistry, and microbiology in continental hydrothermal systems. Astrobiology. 2019;19(12):1505-22.
30. Peacock JP, Cole JK, Murugapiran SK, Dodsworth JA, Fisher JC, Moser DP, et al. Pyrosequencing reveals high-temperature cellulolytic microbial consortia in Great Boiling Spring after in situ lignocellulose enrichment. PLoS One. 2013;8(3):e59927.
31. Hua ZS, Wang YL, Evans PN, Qu YN, Goh KM, Rao YZ, et al. Insights into the ecological roles and evolution of methyl-coenzyme M reductase-containing hot spring Archaea. Nature Communications. 2019;10(1):4574.
32. Wang J, Qu Y-N, Evans PN, Guo Q, Zhou F, Nie M, et al. Evidence for nontraditional *mcr*-containing archaea contributing to biological methanogenesis in geothermal springs. Science Advances. 2023;9(26):eadg6004.
33. Klenk H-P, Clayton RA, Tomb J-F, White O, Nelson KE, Ketchum KA, et al. The complete genome sequence of the hyperthermophilic, sulphate-reducing archaeon *Archaeoglobus fulgidus*. Nature. 1997;390(6658):364-70.
34. Slobodkina G, Allioux M, Merkel A, Cambon-Bonavita MA, Alain K, Jebbar M, et al. Physiological and genomic characterization of a hyperthermophilic archaeon *Archaeoglobus neptunius* sp. nov. isolated from a deep-sea hydrothermal vent warrants the reclassification of the genus *Archaeoglobus*. Frontiers in Microbiology. 2021;12:679245.
35. von Jan M, Lapidus A, Glavina Del Rio T, Copeland A, Tice H, Cheng J-F, et al. Complete genome sequence of *Archaeoglobus profundus* type strain (AV18T). Standards in Genomic Sciences. 2010;2(3):327-46.
36. Anderson I, Risso C, Holmes D, Lucas S, Copeland A, Lapidus A, et al. Complete genome sequence of *Ferroglobus placidus* AEDII12DO. Standards in Genomic Sciences. 2011;5(1):50-60.
37. Mardanov AV, Slododkina GB, Slobodkin AI, Beletsky AV, Gavrilov SN, Kublanov IV, et al. The *Geoglobus acetivorans* genome: Fe (III) reduction, acetate utilization, autotrophic growth, and degradation of aromatic compounds in a hyperthermophilic archaeon. Applied and Environmental Microbiology. 2015;81(3):1003-12.
38. Manzella MP, Holmes DE, Rocheleau JM, Chung A, Reguera G, Kashefi K. The complete genome sequence and emendation of the hyperthermophilic, obligate iron-reducing archaeon "*Geoglobus ahangari*" strain 234T. Standards in Genomic Sciences. 2015;10(1):1-19.
39. Stokke R, Hocking WP, Steinsbu BO, Steen IH. Complete genome sequence of the thermophilic and facultatively chemolithoautotrophic sulfate reducer *Archaeoglobus sulfaticallidus* strain PM70-1T. Genome Announcements. 2013;1(4):e00406-13.
40. Boyd JA, Jungbluth SP, Leu AO, Evans PN, Woodcroft BJ, Chadwick GL, et al. Divergent methyl-coenzyme M reductase genes in a deep-subseafloor Archaeoglobi. The ISME Journal. 2019;13(5):1269-79.
41. Mukherjee S, Seshadri R, Varghese NJ, Eloe-Fadrosh EA, Meier-Kolthoff JP, Göker M, et al. 1,003 reference genomes of bacterial and archaeal isolates expand coverage of the tree of life. Nature Biotechnology. 2017;35(7):676-83.